International Journal of Earth Sciences (2022) 111:2925–2950
https://doi.org/10.1007/s00531-022-02205-1

ORIGINAL PAPER

Exhumation of continental margin rocks from mantle depths to orogenic foreland: example from the Seve Nappe Complex of the central Scandinavian Caledonides

Chong Ma[1,6] · Jarosław Majka[2,3] · Jeffrey A. Benowitz[4] · Christopher Barnes[5] · Håkan Sjöström[2] · David G. Gee[2] · Mark G. Steltenpohl[6]

Received: 4 May 2021 / Accepted: 17 May 2022 / Published online: 17 June 2022

Abstract

The diamond-bearing Seve Nappe Complex (SNC) in the Scandinavian Caledonides records subduction of continental margin rocks to (ultra)high-pressure conditions at mantle depths, and exhumation thereafter from beneath the hinterland to the Earth's surface in the foreland. Structural data of the Upper, Middle, and Lower SNC in central Jämtland, Sweden demonstrate a triclinic bulk deformation during the exhumation of the still ductile SNC from crustal levels where migmatites formed. $^{40}Ar/^{39}Ar$ data from the Upper SNC constrain the timing of cooling through 450−300 °C to be ~ 418 to 416 Ma. In combination with a review of the published pressure–temperature–time data and regional geology of the central Scandinavian Caledonides, four stages of exhumation of the central Jämtland SNC are summarized: (1) buoyancy-driven exhumation during ~ 455 to 433 Ma from ultrahigh-pressure depths to granulite-facies depths triggered by tectonic under-pressure; (2) tectonic exhumation in ~ 433 to 418 Ma at lower- to mid-crustal levels resulted from accretion of the Lower Köli Nappes onto Baltica; (3) eduction of the Western Gneiss Region lithosphere and piggyback transport of the SNC in ~ 418 to 375 Ma from hinterland to foreland, coupled with extensional faulting at mid- to upper-crustal levels; and (4) gravitational collapse- and erosion-driven exhumation following the end of the Scandian Orogeny at ~ 375 Ma. This multi-stage exhumation transported the SNC for > 100 km vertically from mantle depths to the Earth's surface and > 350 km horizontally from the Caledonian hinterland to the foreland. This contribution provides a typical example of the complex exhumation of deeply subducted continental rocks in orogenic belts.

Keywords Scandinavian Caledonides · Seve Nappe Complex · Exhumation of UHP/UP rocks · Structural analysis · $^{40}Ar/^{39}Ar$ geochronology

Introduction

Recognition of coesite and diamond inclusions in garnet, zircon, and/or clinopyroxene (Chopin 1984; Smith 1984; Sobolev and Shatsky 1990) in orogenic belts indicates subduction of crustal rocks to ultrahigh-pressure (UHP) conditions. Exhumation of UHP rocks from depths of > 100 km to the Earth's surface demonstrates an extraordinary tectonic process, but is not yet well understood (e.g., Guillot et al. 2009; Hacker and Gerya 2013; Warren 2013). The Seve Nappe Complex (SNC) in the Middle Allochthon of the Scandinavian Caledonides (Fig. 1) is one of the well-known crustal terranes subducted to high-pressure (HP) and UHP conditions. Regional occurrences of eclogites, garnet pyroxenite, garnet peridotites (e.g., Brueckner et al. 2004; Janák et al. 2013; Majka et al. 2014a; Gilio et al. 2015; Klonowska

✉ Chong Ma
macmachong@gmail.com

1 Harquail School of Earth Sciences, Laurentian University, Sudbury, ON P3E2C6, Canada

2 Department of Earth Sciences, Uppsala University, 752-36 Uppsala, Sweden

3 Geophysics and Environmental Protection, Faculty of Geology, AGH University of Science and Technology, 30-059 Kraków, Poland

4 Geophysical Institute, University of Alaska, Fairbanks, AK 99775, USA

5 Institute of Geological Sciences, Polish Academy of Sciences, 31-002 Krakow, Poland

6 Department of Geosciences, Auburn University, Auburn, AL 36830, USA

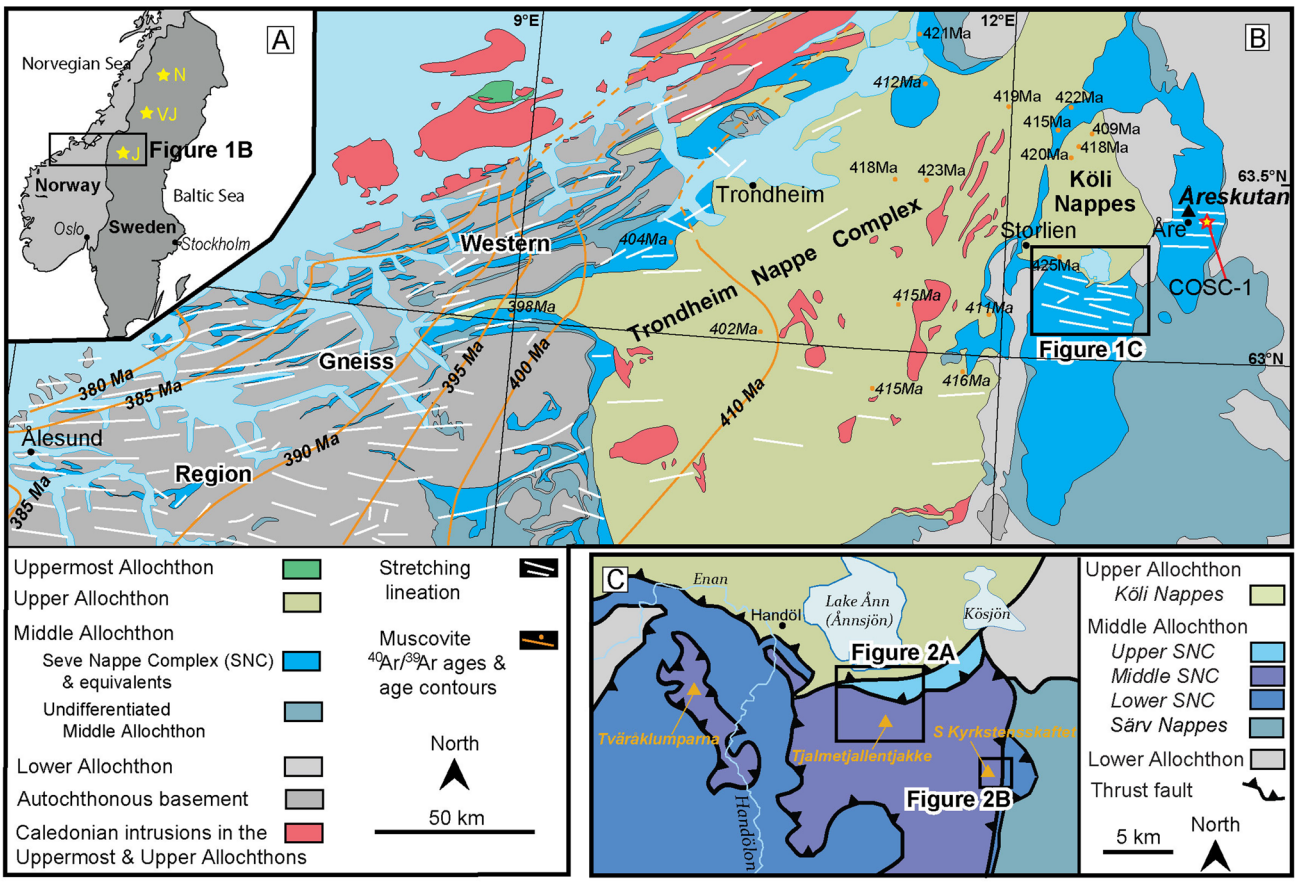

Fig. 1 Simplified Geological maps of the central Scandinavian Caledonides (**A**, **B**) (Solli and Nordgulen 2008) and central Jämtland (**C**) showing the study areas. The contours of $^{40}Ar/^{39}Ar$ age are from Walsh et al. (2013). Other muscovite $^{40}Ar/^{39}Ar$ ages are from Dallmeyer et al. (1985), Dallmeyer (1990), and Hacker and Gans (2005). Regional stretching lineations are from Seranne (1992), Hacker and Gans (2005), and Hacker et al. (2010). *N* Norrbotten, *VJ* southern Västerbotten and northern Jämtland, *J* central Jämtland, *COSC-1* Collisional Orogeny in the Scandinavian Caledonides scientific drilling hole (Gee et al. 2010)

et al. 2016; Bukała et al. 2018), and metamorphic microdiamonds (Majka et al. 2014b; Klonowska et al. 2017; Janák et al. 2017) in the SNC from southern Norrbotten to central Jämtland, Sweden (Fig. 1A) suggests a large HP/UHP metamorphic belt (> 400 km north–south) along the orogenic foreland. The SNC is considered to be derived from the Baltoscandian continental outer margin and continent-ocean transition zone, based on its metasedimentary and mafic magma-rich protoliths (Andréasson 1994; Andréasson et al. 1998; Jakob et al. 2019), the latter of early Ediacaran (ca. 600 Ma) age (Svenningsen 2001; Gee et al. 2013). Considering its current position in the Caledonian foreland above the low-grade sedimentary rocks of the Baltoscandian foreland, the SNC documents a prolonged history from the extension of the Baltica continental margin, through deep subduction beneath Cambrian to earliest Ordovician oceanic crust, to exhumation and accretion along the Baltoscandian margin, followed by transport from the hinterland to the foreland (e.g., Gee 1978; Gee et al. 2020).

Abundant pressure–temperature–time (P–T–t) data became available recently for the SNC, related to Ordovician subduction during Iapetus closure, with conditions of up to 2.3−4.2 GPa in ~ 483 to 455 Ma (Stephens and Van Roermund 1984; Andréasson et al. 1985; van Roermund 1985, 1989; Albrecht 2000; Brueckner et al. 2004; Brueckner and van Roermund 2007; Janák et al. 2013, 2017; Klonowska et al. 2014, 2016, 2017; Majka et al. 2014b; Andersson 2015; Fassmer et al. 2017; Bukała et al. 2018; Walczak et al. 2019, 2022). In central Jämtland, the HP to UHP metamorphism was followed by a high-temperature (850−860 °C), lower-pressure event resulting in migmatization at ~ 445 to 435 Ma (Gromet et al. 1996; Majka et al. 2012; Ladenberger et al. 2014; Klonowska et al. 2017; Walczak et al. 2019, 2022). These data provide important constraints on the exhumation of the SNC from HP/UHP to migmatization conditions. The exhumation thereafter through crustal levels, including eastward transport of the

allochthons for several hundred kilometers onto the Baltoscandian platform, however, remains elusive.

This contribution reports new structural and $^{40}Ar/^{39}Ar$ data associated with the exhumation of the central Jämtland SNC following the ~ 445 to 435 Ma migmatization event, and synthesizes literature data providing orogenic scale constraints on the exhumation of the SNC. The goals are to provide a comprehensive view of the exhumation of the SNC in the central Scandinavian Caledonides (Fig. 1B) from mantle depths beneath the Caledonian hinterland to the Earth's surface above the foreland, and to provide insights into the general processes of exhumation of deeply subducted continental rocks in orogenic belts.

Tectonostratigraphy of the central Scandinavian Caledonides

The central Scandinavian Caledonides is characterized by large thrust sheets of continental or oceanic origins, all emplaced eastwards onto the Baltoscandian platform (Gee 1975, 1978) of the Baltic Shield that largely consists of the Paleoproterozoic Svecokarelian orogen and Late Paleoproterozoic Transscandinavian Igneous Belt (e.g., Gorbatschev 1985). Four groups of nappes have been defined (Gee et al. 1985, with subsequent minor modification), the Lower, Middle, Upper, and Uppermost allochthons. The Lower has been inferred to be derived from the Baltoscandian platform and inner margin, the Middle from the outer margin and continent-ocean transition zone, the Upper from the Iapetus Ocean, and the Uppermost from the Laurentian continental margin. Descriptions of these allochthons and interpretations of their origins have been widely discussed, with numerous contributions during the last forty years, from Gee and Sturt (1985) to those in Corfu et al. (2014) and the subsequent discovery of widespread UHP. In the study area of the central Scandinavian Caledonides (Fig. 1B, Gee 1975), the Uppermost Allochthon (Roberts et al. 2007 and references therein), representing Laurentian margin, is not preserved. The Upper Allochthon (i.e., the Köli Nappes) is mostly composed of greenschist-facies assemblages (Beckholmen 1982; Sjöström 1984) including Early Ordovician (and perhaps late Cambrian) oceanic crust, for examples the Handöl (Bergman 1993) and Raudfjellet (Nilsson et al. 2005) ophiolites, island-arc/forearc/backarc lithologies, and deep-water sediments (Gee et al. 2014). Structurally below these Iapetus-related nappes is the SNC (included in the Middle Allochthon, Gee et al. 2008), representing the outer and outmost magma-rich margin of western Baltica (Andréasson 1994; Gee et al. 2013; Andersen et al. 2022). The underlying Jämtland Supergroup of the Lower Allochthon comprises Proterozoic basement-derived thrust sheets and overlying Neoproterozoic rifted margin, Ediacaran–Cambrian passive margin, and Ordovician–Silurian foreland basin successions (Gee 1975). These allochthons are separated by a major décollement from footwall Cambrian alum shale on the top of the underlying autochthon, the latter dominated by Precambrian crystalline basement rocks commonly with overlying thin quartzites (Gee et al. 2014). In western Sweden, the metamorphic grade of the allochthons increases upwards from low greenschist-facies in the Lower Allochthon to amphibolite-, granulite-, and eclogite-facies in the top of the Middle Allochthon (Sjöström 1984). The latter contrasts markedly with the greenschist-facies and, locally lowest amphibolite-facies Köli Nappes of the Upper Allochthon (Bergman 1993). The Scandinavian nappe pile is up to several kilometers thick and vast in areal distribution (up to 100 s km wide and > 1000 km long) with a general decrease in thickness towards the hinterland in western Norway, particularly notable in the Middle Allochthon (Gee et al. 2010, 2013).

The Middle Allochthon, the focus of this study, was assembled by thrusting of nappes with distinctive protoliths and metamorphic grades. From top to bottom, the high-grade SNC overlies the Särv Nappes that consist of upper greenschist-facies metamorphosed thick feldspathic sandstones and subordinate carbonates and tillites, all intruded by rift-related dolerite dykes (Strömberg 1961; Arnbom 1980; Be'eri-Shlevi et al. 2011; Andersen et al. 2012) of Ediacaran age (ca. 600 Ma, Kjøll et al. 2019). The Särv Nappes were thrust as a mainly rigid duplex (Gilotti and Kumpulainen 1986) along a basal mylonite zone onto a basement-derived allochthon, the Tännäs Auguen Gneiss Nappe (Röshoff 1978); farther north this footwall comprises feldspathic sandstones and minor conglomerates of the Offerdal Nappe (Gee et al. 2014). The initial stacking of these Middle allochthons may have occurred in the Ordovician, providing the source for the westerly derived, Middle Ordovician turbidites of the foreland basin (Karis in Karis and Strömberg 1998). The Middle allochthons in the Åre and Offerdal synforms of central Jämtland overlie the Llandovery turbidites and conglomerates of the Änge group (Kulling 1933; Gee et al. 2014), which constrains the timing of Scandian emplacement of the overlying allochthons to be post ca. 433 Ma.

The distance of thrusting of the Middle Allochthon, from hinterland to foreland, was inferred to be over 100 km by Törnebohm (1888). Subsequent studies provided evidence of much greater distances of > 350 km (e.g., Gee 1975, 1978; Nystuen et al. 2008; Gee et al. 2017, 2020) or of > 1200 km if the pre-Caledonian margin of Baltica was hyperextended (e.g., Andersen et al. 2012, 2022; Jakob et al. 2019). The major lines of evidence supporting long-distance thrusting of these nappes include: (1) the Archean–Proterozoic Baltica basement of the autochthon-paraautochthon extends from the Caledonian front in Sweden to the Norwegian coast (Gee et al. 2010); (2) the magnetic anomalies (e.g., Dyrelius

1985) related to the autochthonous basement can likewise be followed from the autochthon to the west coast; (3) the Baltoscandian platform-cover sediments (e.g., Andersson et al. 1985) represented by Ediacaran−Cambrian quartzites and Cambrian alum shales (organic-rich; high uranium, vanadium, molybdenum, and nickel) crop out from the Caledonian front to the hinterland windows in Tömmerås and Trollheimen; (4) the Särv Nappes dolerite dyke-swarms are not present in the underlying allochthons east of Trondheimsfjord; and there, only in the underlying augen gneisses; (5) subduction-related SNC with felsic intrusions has recorded much higher P–T conditions (e.g., Klonowska et al. 2017) than any underlying nappe in the hinterland to the east of the Western Gneiss Region, where the metamorphism of the Lower allochthons reaches UHP conditions and is of Early Devonian age. Thus, the dyke-intruded thrust sheets in the Middle Allochthon (SNC and Särv Nappes) and overlying Upper and Uppermost allochthons, must have been transported more than 350 km towards the foreland onto the Baltoscandian platform, with initial displacements during Ordovician accretion and subsequent thrusting during Scandian continent–continent collision.

Seve Nappe Complex in central Jämtland, Sweden

Regional framework

The SNC in western Sweden is dominated by psammitic and pelitic schists and gneisses with subordinate marbles, calc-silicate gneisses, amphibolitized dolerites and gabbros, and minor eclogites and peridotites (e.g., Zachrisson 1973; Ladenberger et al. 2014). The similarity in protolith of the Lower SNC and the Särv Nappes from Jämtland to Norrbotten (Fig. 1A), with similar aged mafic dykes and a dominance of 1800−900 Ma detrital zircons in the psammitic gneisses and schists (Gee et al. 2014), are consistent with the Neoproterozoic rift setting along the Baltica margin (Kjøll et al. 2019). The youngest detrital zircons of 726 ± 20 Ma and 811 ± 23 Ma (2σ) from two metapsammite samples of the SNC, respectively (Kirkland et al. 2011), suggest that some of the protoliths were deposited during the Cryogenian or early Ediacaran (Gee et al. 2013). Likewise, some of the SNC paragneisses share detrital zircon age-spectra with some of the Neoproterozoic rift strata of the Särv Nappes (Be'eri-Shlevin et al. 2011) that were deposited during the Neoproterozoic rifting (Kumpulainen 1980). Therefore, the depositional age of the metasedimentary protoliths of the SNC is inferred to be broadly coeval with the Neoproterozoic continent rifting that led to the opening of the Iapetus Ocean (e.g., Andersen et al. 2012; Jakob et al. 2019; Gee et al. 2020).

HP/UHP metamorphism is recorded in the Lower and Middle SNC at several locations along the orogen. In southern Norrbotten (Fig. 1A), HP (1.5–3.1 GPa, 610–780 °C) eclogite, garnet pyroxenite, and associated paragneiss of the Vaimok Lens (equivalent of the Lower SNC) (Stephens and Van Roermund 1984; Andréasson et al. 1985; van Roermund 1989; Albrecht 2000; Bukała et al. 2018) yielded a monazite rim Th–U–Pb age of 498 ± 10 Ma (Barnes et al. 2019), titanite U–Pb ages of ca. 500–475 Ma (Essex et al. 1997), and zircon U–Pb ages of 482 ± 1 Ma (Root and Corfu 2012) and ca. 480–475 Ma (Barnes et al. 2019). About 300 km to the south in southern Västerbotten and northern Jämtland (Fig. 1A), HP/UHP (2.3–4.0 GPa, 750–960 °C) eclogite, garnet pyroxenite, garnet peridotite, and microdiamond are documented in the Middle and Lower SNC (van Roermund 1985; 1989; Brueckner et al. 2004; Janák et al. 2013, 2017; Majka et al. 2014a; Klonowska et al. 2016). The timing of HP/UHP metamorphism in this area is constrained to be ca. 460 Ma based on a weighted mean of mineral Sm–Nd isochron ages of 458 ± 5 Ma (Brueckner and van Roermund 2007), zircon rim U–Pb ages of ca. 460 Ma (Andersson 2015) and 459 ± 3 Ma (Fassmer et al. 2017), and a garnet-whole rock Lu–Hf age of 459 ± 1 Ma (Fassmer et al. 2017). About 250 km further to the south in central Jämtland (Fig. 1A), UHP metamorphism (4.1–4.2 GPa, 830–840 °C) is reported in the Middle SNC from kyanite–garnet migmatitic paragneiss of Åreskutan (Fig. 1B), which is corroborated by occurrences of metamorphic microdiamond at Åreskutan and Tväråklumparna (Fig. 1C) (Majka et al. 2014b; Klonowska et al. 2014, 2017). The timing of UHP in central Jämtland is interpreted to be 483 ± 4 Ma (Walczak et al. 2022) on the basis of U–Pb data from metamorphic zircon overgrowths in the diamond-bearing gneiss at Tväråklumparna (Majka et al. 2014b). The HP condition was likely maintained to 455 ± 11 Ma based on a monazite U-Th-Pb age at Åreskutan (Majka et al. 2012). Migmatization following the HP/UHP metamorphism occurred widely in the Middle SNC and is characterized by granulite-facies assemblages in rocks of pelitic composition (Gee et al. 2013). This high-temperature (850–860 °C) melting event has been constrained to be ca. 445–435 Ma by zircon and monazite U–Pb ages (Gromet et al. 1996; Ladenberger et al. 2014; Klonowska et al. 2017; Walczak et al. 2019, 2022).

The formation of HP/UHP parageneses in the SNC is considered to result from subduction of the SNC beneath the Iapetus oceanic lithosphere that is partially preserved in the Köli Nappes of the Upper Allochthon (e.g., Majka et al. 2014b). The plutonic and volcanic island-arc assemblages of the Upper, Middle, and Lower Köli Nappes range in age from late Cambrian to Late Ordovician, which suggests that subduction in the Iapetus Ocean was active throughout the Ordovician (Gee 2015). In the Upper Köli Nappes, late Cambrian to Early Ordovician ophiolites are overlain by Early to

Middle Ordovician limestones with fossils of North American affinity (Bruton et al. 1985), which indicates that these oceanic crust fragments were obducted before or during the Early Ordovician, and that the obduction of this oceanic crust was proximal to the Laurentian margin. Above the obducted Lower Köli oceanic crust (e.g., the Vågåmo ophiolite, Sturt et al. 1991), detrital serpentinites were deposited and included a fauna of Early–Middle Ordovician age with mixed Baltica-North American affinities (Harper et al. 2008). Above the detrital serpentinites in the succession, Late Ordovician quartzites contain Baltica-derived detrital zircons (Gee et al. 2014). Therefore, the Lower Köli ophiolite was obducted proximal to the Baltic margin. Following emplacement of ophiolites and/or plutons in the Upper, Middle, and Lower Köli, turbidites, shales, conglomerates, sandstones, limestones, and/or volcaniclastics were deposited and some of them are as young as early Silurian in the Lower and Middle Köli (Gee 2015). This suggests that the Middle Köli was not yet stacked on the Lower Köli and the latter was not yet emplaced onto Baltica until early Silurian. Since the Lower Köli was proximal to the Baltic margin in the Late Ordovician (Gee et al. 2014), the formation of HP/UHP parageneses in the SNC was probably due to subduction of the SNC beneath an oceanic terrane represented by the Lower Köli Nappes. This interpretation is consistent with the condition that the Handöl ophiolite in Sweden (Bergman 1993) and the Raudfjellet ophiolite in Norway (Nilsson et al. 2005) at the base of the Lower Köli Nappes are directly underlain by the high-grade SNC.

In central Jämtland, the SNC is subdivided into three units, i.e., Upper, Middle, and Lower SNC. The Upper SNC is represented by highly strained kyanite-bearing garnet-mica schists and amphibolites (Sjöström 1984; Bergman 1992). The Middle SNC (e.g., Åreskutan Nappe) is characterized by granulite-facies migmatites and migmatitic gneisses, kyanite- and sillimanite-bearing paragneisses, leucogranite, and metamorphosed mafic dykes (e.g., Arnbom 1980; Ladenberger et al. 2014). The Lower SNC is largely composed of amphibolite-facies metapsammites, mica schist, calc-silicate gneisses, marbles, amphibolites, and locally metadolerites and ultramafites, which are locally overprinted by greenschist-facies retrogression (e.g., Gee et al. 2014; Klonowska et al. 2017).

Lithologies of the Seve Nappe Complex near Lake Ånn

Detailed mapping was conducted by the current study in two areas (Fig. 1C) to the south of Lake Ånn in central Jämtland between the diamond-bearing outcrops at Tväråklumparna and Åreskutan. The western area (Fig. 2A) was chosen for exposures of the Upper and Middle SNC, and the eastern area (Fig. 2B) for the Middle and Lower SNC.

In general, the Upper and Middle SNC are compositionally similar and continuous; the major difference lies in the degree of strain accumulated, i.e., distinctively higher strain in the Upper SNC indicated by more continuous foliation and finer-grained porphyroclasts and/or porphyroblasts. The Upper SNC is composed of protomylonitic−mylonitic (kyanite-)sillimanite-garnet-biotite quartzofeldspathic gneiss, garnet amphibolite, calc-silicate gneiss, and a mylonite−ultramylonite roof shear zone (80−120 m thick) of (kyanite-)garnet-muscovite-biotite quartzofeldspathic gneiss/schist immediately beneath the Köli Nappes (Fig. 2A). Synkinematic muscovite flakes (up to 3 cm) characteristically define the foliation of the roof shear zone. The Middle SNC comprises (kyanite-) sillimanite-garnet-biotite quartzofeldspathic gneiss and migmatite along with garnet amphibolite and calc-silicate gneiss (Fig. 2). Rocks at the base of the Middle SNC are deformed to protomylonites and mylonites above a thrust (Fig. 2B). Immediately underlying the basal thrust of the Middle SNC, poorly exposed rocks of the Lower SNC (amphibolite, muscovite-metapsammite, and calc-silicate gneiss) exhibit mylonite−ultramylonite fabrics (Fig. 2B). Phyllite and schist also occur in the Lower SNC further east according to regional geologic maps (e.g., Sjöstrand 1999).

The migmatite of the Middle SNC features leucosomes containing coarse-grained garnet in a quartzofeldspathic matrix and paleosomes of mostly biotite, finer-grained garnet, and sillimanite (Fig. 3A). Some sillimanite crystals are > 7 cm long. Two phases of garnet growth are recognized in the leucosome; dark-rose garnets (grt I) are overgrown by a much more common, light-rose phase (grt II). The two generations of garnet form core-and-mantle, clasts-in-matrix, or complete replacement structures (Fig. 3B). Large (~ 12 by 2 cm) kyanite grains showing stable contacts to the dark-rose garnets (Fig. 3C,D), kyanite overgrown by sillimanite (Fig. 3E), and radial fractures in garnet around quartz inclusions suggesting former presence of coesite (Fig. 3F) are collectively consistent with the interpretation of (U)HP metamorphism overprinted by a high-temperature event in the SNC. The growth of sillimanite due to the high-temperature event was polyphase, which is indicated by sillimanite of different generations in migmatite of the Middle SNC (Fig. 3G).

Biotite-muscovite pegmatitic dykes and pods are widespread in the mapped SNC. Most show no deformation as indicated by euhedral micas up to 6 cm across, whereas some pegmatites are strained into lens-shaped blocks containing euhedral minerals. Amphibolitized mafic dykes are also common and extensively stretched or variously strained. In short, the Upper, Middle, and Lower SNC in the study area are compositionally consistent with passive margin sequences intruded by mafic dykes that have collectively been overprinted by high-grade metamorphism, partial

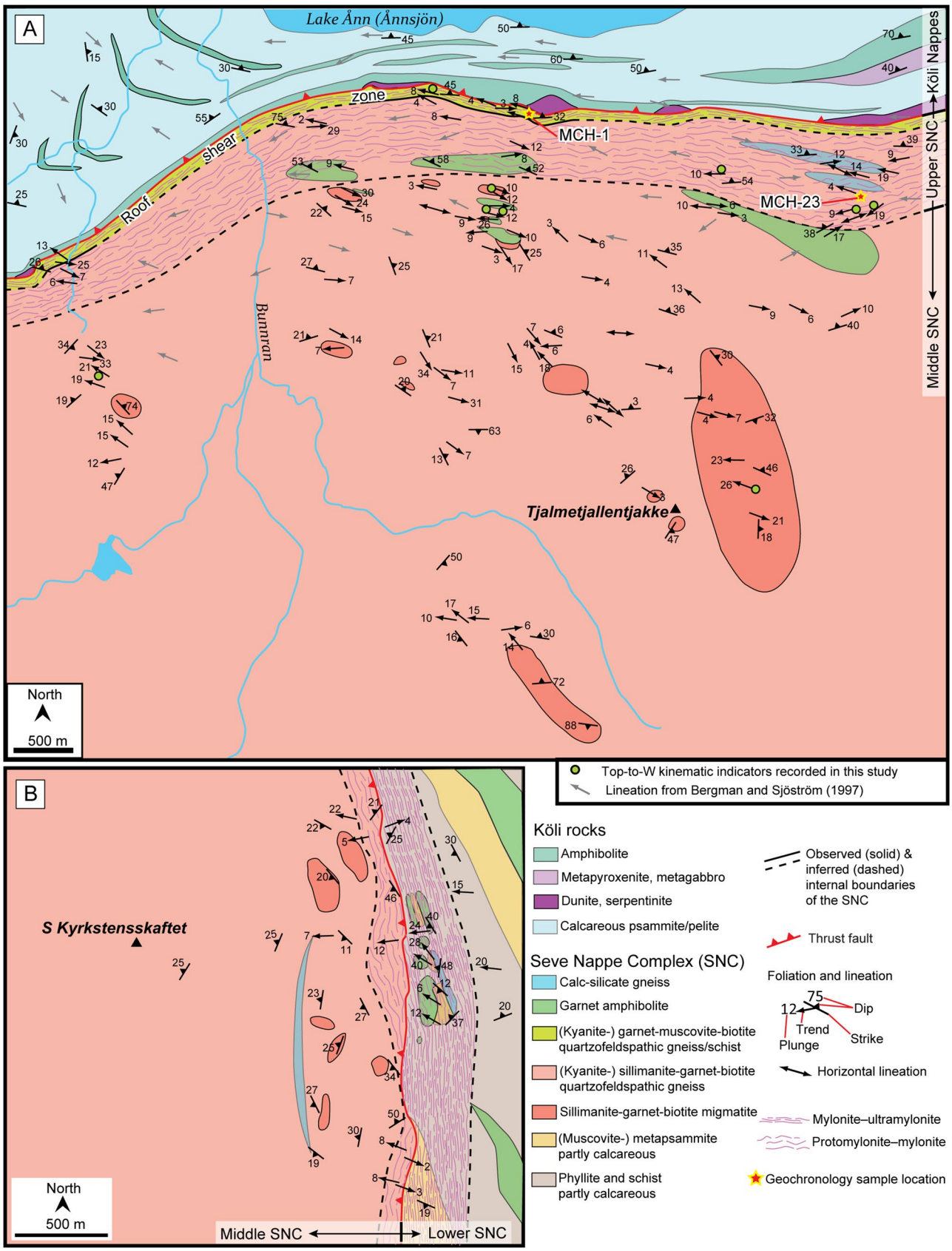

Fig. 2 Geologic map of the western (**A**) and eastern study area (**B**) with representative structural data. See map locations in Fig. 1C and detailed maps in Figure S1

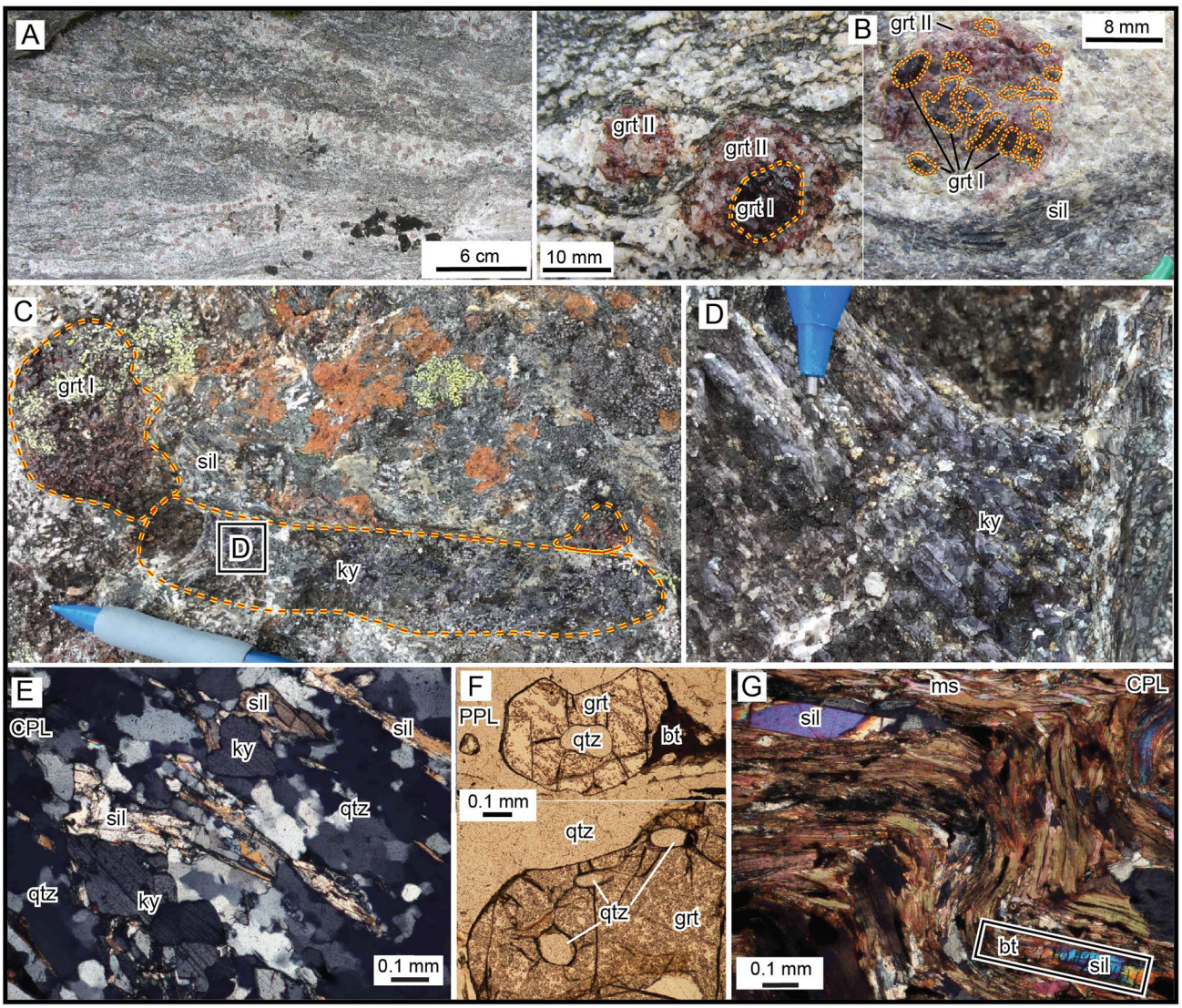

Fig. 3 Representative lithologies of the Seve Nappe Complex. **A** Migmatite with leucosome containing coarse-grained garnet and sillimanite. **B** Two generations of rose garnet (grt-I: dark and older; grt-II: light and younger). **C** Large kyanite (a closer look in **D**) in equilibrium with the dark-rose garnets. **E** Thin-section of kyanite-sillimanite-bearing gneiss. **F** Microphotograph showing quartz inclusions in garnet surrounded by radial fractures suggesting breakdown of former coesites. **G** Microfolds defined by sillimanite and biotite in the paleosome of a migmatite. Note that the sillimanite outlined by the box is strained and show transition to biotite in the same grain whereas the sillimanite at upper left is strain-free and has sharp contact to biotite, which suggests two generations of sillimanite. *bt* biotite, *grt* garnet, *ky* kyanite, *ms* muscovite, *qtz* quartz, *sil* sillimanite, *PPL* plane polarized light, *CPL* cross polarized light

melting, and pervasive poly-deformation that is described below.

Ductile structures of the Seve Nappe Complex near Lake Ånn

Generations of fabrics

Three generations of ductile fabrics are distinguished in the current study based on crosscutting relationships. For example, blocks of pre-migmatization elliptical and planar fabrics are enclosed in migmatite that in turn is overprinted by ductile shear fabrics. The most distinctive fabric is the alternating mafic and felsic layers in the Middle SNC migmatite, including planar, discordant (Fig. 4A), and folded foliations (in both mesoscale and microscale, Fig. 4B). The mesoscale folds are tight to isoclinal and commonly rootless (Fig. 4B). Within the migmatite, garnet-amphibolite lenses and sporadic blocks of paragneiss paleosome contain discordant foliations and rare kyanite. Development of a partially melted zone in some of the blocks (Fig. 4C) suggests that these predate migmatization and that their fabrics are

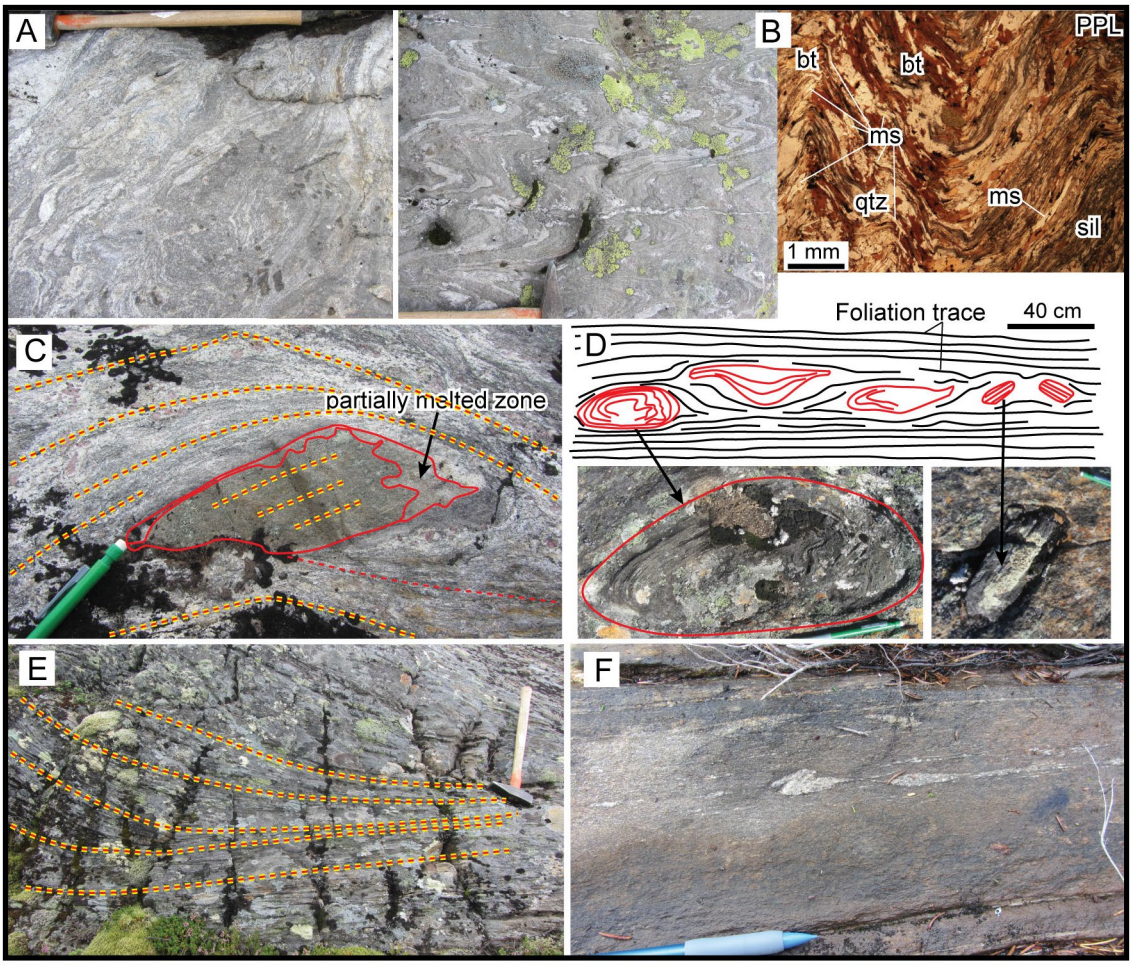

Fig. 4 Typical fabrics of the Seve Nappe Complex (SNC). **A** Planar and discordant migmatitic foliations. **B** Folded migmatitic foliations in the mesoscale (left) and microscale (right). **C** Isolated block containing discordant foliations and a partially melted zone surrounded by migmatite. **D** Isolated blocks of elliptically and randomly orientated foliations enclosed in migmatite. **E** Ductile shear fabrics in the Middle SNC. **F** Ultramylonitic fabrics in the Upper SNC. *bt* biotite, *ms* muscovite, *qtz* quartz, *sil* sillimanite, *PPL* plane polarized light

older than those in the migmatite. Elliptically and randomly orientated foliations of the paragneiss blocks (Fig. 4D) further indicate the existence of earlier fabrics. The migmatitic fabrics are commonly modified by ductile shear (Fig. 4E) resulting in gneissic, schistic, or mylonitic fabrics (Fig. 4F). This modification might have obliterated many original migmatite fabrics formed during the high-temperature event at about 440 Ma in the Middle SNC (e.g., Ladenberger et al. 2014).

S-L fabrics

The foliation and lineation associated with the ductile shear following the migmatization of the SNC are characterized by crystal-plastic deformation indicative of relatively high-temperature conditions. Elevated temperatures are demonstrated by the occurrence of gneissic fabrics, microstructures in quartz and feldspar, and mineralogy of sheared rocks.

In the Upper SNC, dynamically recrystallized quartz shows lobate and amoeboid grain boundaries (Fig. 5A), typical of grain boundary migration (Passchier and Trouw 2005). Quartz ribbons enclosing garnets and defining the mylonitic foliation have strain-free grains showing polygonal and straight boundaries with interfacial angles of ~ 120° (Fig. 5B). The latter suggests grain boundary area reduction for decreasing energy during and/or following high-temperature deformation (Passchier and Trouw, 2005). In the shear zones within the Middle SNC, quartz is generally recrystallized by grain boundary migration (Fig. 5C) and some feldspar twins are bended (Fig. 5D). In the shear zones of the Upper and Middle SNC, stable (i.e., no retrogression) amphibole and garnet occur along the ductile lineation and new sillimanite was crystallized along the mylonitic foliation. These lines of evidence collectively suggest high-temperature conditions during ductile shear of the SNC after the migmatization event.

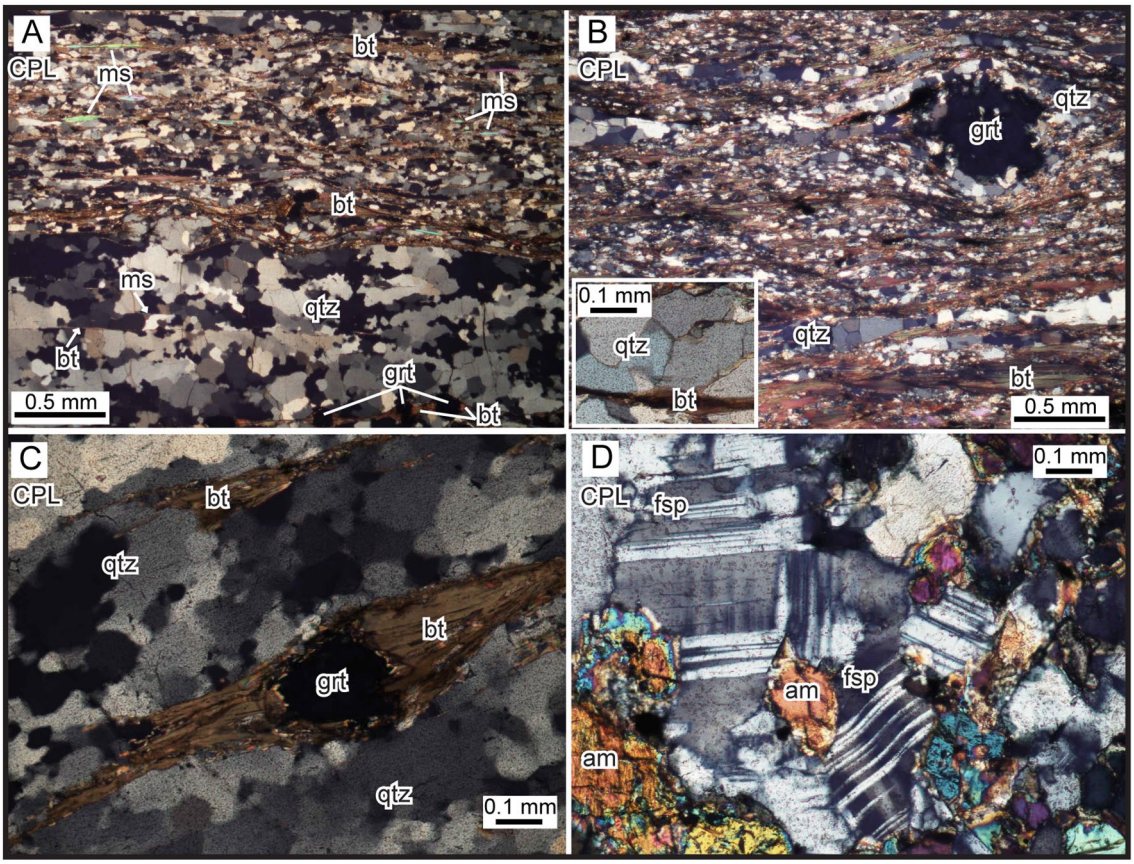

Fig. 5 Microphotographs showing microstructures of quartz and feldspar. **A** Lobate and amoeboid grain boundaries of quartz in the Upper Seve Nappe Complex (SNC). **B** Quartz ribbons showing strain-free grains with polygonal and straight boundaries of ~ 120° interfacial angles in the Upper SNC. **C** Quartz recrystallized by grain boundary migration in the Middle SNC. **D** Bended feldspar twins in the Middle SNC. *am* = amphibole, *bt* biotite, *fsp* feldspar, grt garnet, *ms* muscovite, *qtz* quartz, *CPL* cross polarized light

The foliation is generally defined by (re)crystallized mica and quartz in schist and alternating mafic and felsic layers in migmatite and gneiss. The lineation is commonly characterized by ductile ridge-in-groove lineation (Lin et al. 2007) defined by quartz, feldspar, biotite, and/or amphibole along with preferred orientation of newly grown muscovite, quartz, and/or sillimanite.

In general, from the top of the Upper SNC to the interior of the Middle SNC, foliations get shallower and are less consistently oriented (Fig. 6a−6c, stereoplots i). In the roof shear zone of the Upper SNC, the mylonitic foliations strike E-W and dip moderately to the north with limited variation along and across the length of the unit (Fig. 6a, stereoplot i). In the remaining part of the mapped Upper SNC, the foliations (gneissosity overprinted by mylonitic foliations) strike mostly E–W, locally NW–SE and NE–SW, with a moderate to shallow dip to the north (Fig. 6b, stereoplot i). In the Middle SNC, migmatitic layers and gneissosity are overprinted at several structural levels by mylonitic foliations that are subhorizontal and related to shear zones. Outside of these shear zones, steep migmatitic foliations of various attitudes are common (Fig. 6c, d, stereoplots i). Foliations in the Lower SNC are defined by schistosity and gneissosity overprinted by mylonitic foliations, and dip shallowly to the west or WSW (Fig. 6e, stereoplots i). These fabrics are concordant with the mylonitic foliations of the Middle SNC immediately above (Fig. 6d, stereoplots i).

The lineations (Fig. 6a−e, stereoplots ii) are shallowly-plunging in gently folded rocks and generally subhorizontal in planar and isoclinally folded zones. The lineation largely trends between E–W and ESE–WNW.

Kinematics of deformation

The post-migmatization ductile shear of the SNC rocks was strongly partitioned into rheologically different lithologies as shown by distinctive fabrics of adjacent rock units (Fig. 7A). Ductile ridge-in-groove lineations and sheath folds with fold axes parallel to the lineation are commonly well-developed (Fig. 7B,C). The sense of shear is revealed by kinematic indicators appearing on the plane perpendicular to the foliation and parallel to the lineation. Top-to-ESE and top-to-WNW

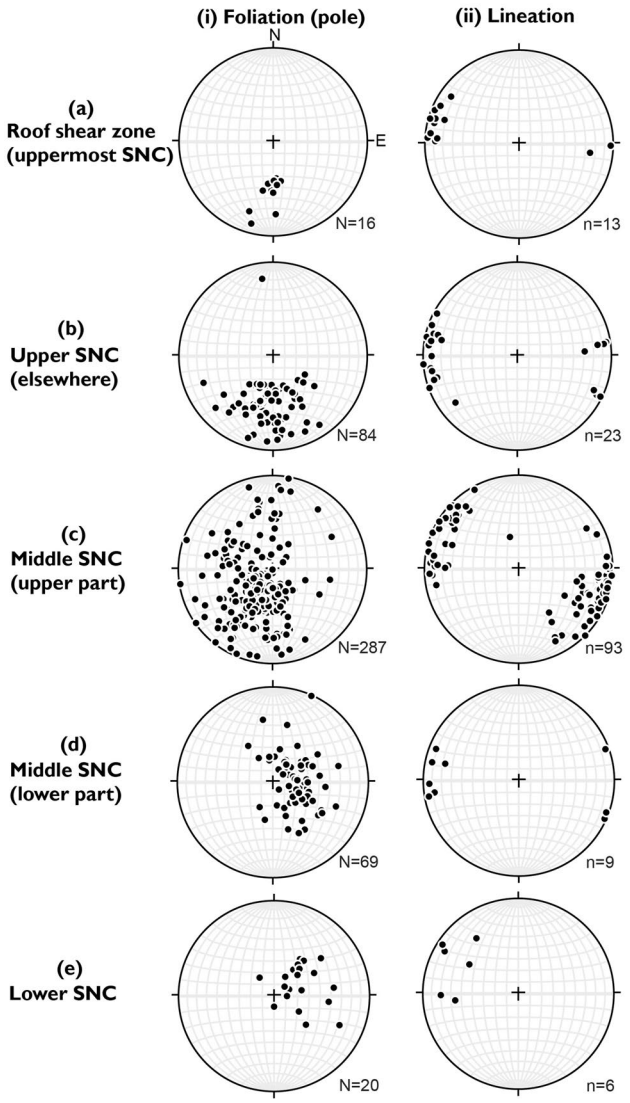

Fig. 6 Structural data of foliations and lineations from various structural levels of the Seve Nappe Complex (SNC), equal-area lower hemisphere projection

shear both occur but the former is predominant. In the mesoscale, widespread sigma-porphyroclasts and S-C structures in garnet amphibolites (Fig. 7D) and migmatitic gneisses (Fig. 7E), sigma-porphyroclasts of felsic melt pods in schists (Fig. 7F), and pervasive S-C structures in metapsammites (Fig. 7G) all indicate a dominant top-to-ESE shear. Top-to-WNW shear indicators occur at a few localities (Fig. 2A) where they are well-developed as sigma-porphyroclasts, S-C structures, and asymmetric blocks (Fig. 7H, I).

In the microscale, the pervasive top-to-ESE shear is recorded by mica fish, S-C structures, delta-porphyroclasts, sigma-porphyroclasts, and shear bands (Fig. 8A–C). The top-to-WNW shear is documented mostly by S-C structures and asymmetric porphyroclasts (e.g., Fig. 8D,E).

Coexistence of top-to-ESE and top-to-WNW shear has been observed in multiple samples. In a thin-section of sillimanite-garnet-biotite quartzofeldspathic gneiss from the lower part of the Upper SNC, biotite and quartz are arranged in S-C structures with opposite senses of shear at a distance of ~ 2 mm (Fig. 8D). In another thin-section of garnet-muscovite-biotite quartzofeldspathic schist from the roof shear zone of the Upper SNC, biotite and garnet form a winged porphyroclast indicating top-to-WNW shear and, along the adjacent foliations, biotite, sillimanite, and muscovite show a S-C structure of top-to-ESE shear (Fig. 8E).

In short, the kinematic indicators preserved in the SNC show a dominant top-to-ESE shear locally accompanied by a top-to-WNW shear. The fabrics displaying opposite kinematics are concordant without overprinting and/or crosscutting relationships and are broadly similar in metamorphic grade.

Structures that accommodated the mass transport along the shear direction probably include boudins and faults in both mesoscale and microscale along with intergranular and intragranular shear in the microscale. The most common boudins in the SNC are amphibolite blocks formed by flattening and stretching of mafic dykes. An estimate of a minimum amount of stretch of 315% was obtained from a representative boudinaged dyke (Fig. 9A). Foliation-parallel sliding combined with foliation-oblique thrusting along a fault at the bottom of the Middle SNC (Fig. 9B) suggests that foreland-directed faults have contributed to the mass transport.

Structures in lineation-normal plane

Structures exposed in the surface perpendicular to lineation help reveal the three-dimensional structures associated with the ductile shear of the SNC. On this plane, some of the sheath folds are flattened (Fig. 10A) and symmetric blocks of felsic melt show a typical boudinage geometry (Fig. 10B). In the same plane, asymmetric blocks (Fig. 10C) and shear bands in the Middle SNC immediately beneath the Upper SNC in the western area (Fig. 2A) show top-to-NNE shear, whereas S-C structures (Fig. 10D) in the Middle SNC immediately above the Lower SNC in the eastern area (Fig. 2B) demonstrate top-to-SSW shear. Gentle, large (100 s m-scale, Fig. 10E) and tight, small (cm-scale, Fig. 10F) folds are recorded in the lineation-normal plane as well. These folds have steep axial surfaces striking parallel to the trend of the lineation.

$^{40}Ar/^{39}Ar$ thermochronology

Samples and analytical methods

Muscovite, biotite, and potassium-feldspar from two rocks were analyzed for $^{40}Ar/^{39}Ar$ geochronology. The sample

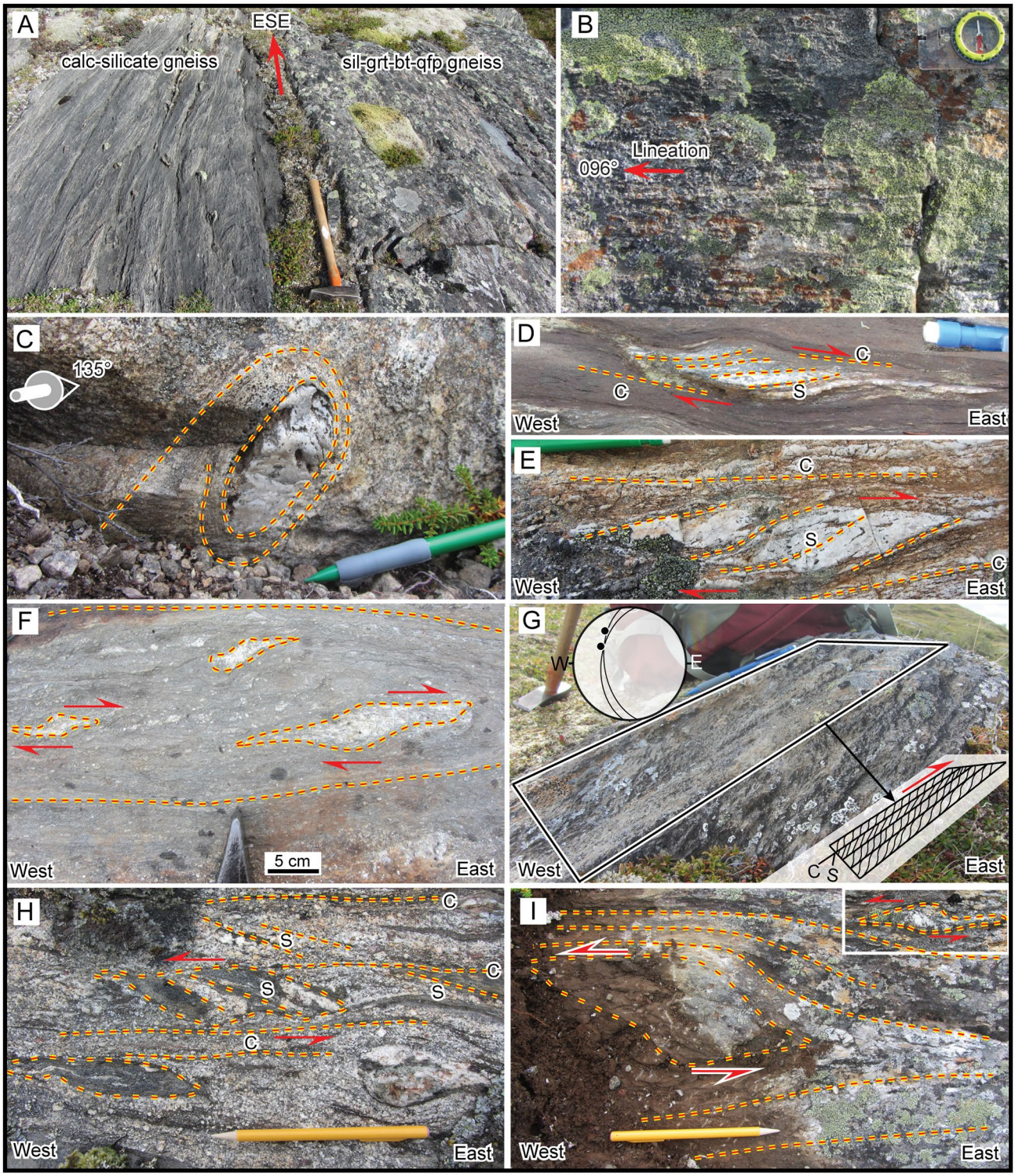

Fig. 7 Outcrop structures on lineation-parallel planes associated with the post-migmatization ductile deformation of the Seve Nappe Complex. **A** Strain partitioning between calc-silicate gneiss and sillimanite-garnet-biotite quartzofeldspathic gneiss (sil-grt-bt-qfp gneiss). **B** Well-developed ductile ridge-in-groove lineations trending E–W in sillimanite-garnet-biotite quartzofeldspathic gneiss. **C** Sheath folds with axes parallel to the lineation. **D–G** Asymmetric porphyroclasts/blocks, S-C structures, and sigma-porphyroclasts showing top-to-ESE shear (to the right in photographs) on the plane perpendicular to the foliation and parallel to the lineation. **H–I** Asymmetric blocks, S-C structures, and sigma-porphyroclasts showing top-to-WNW shear (to the left in the photographs) on the plane perpendicular to the foliation and parallel to the lineation

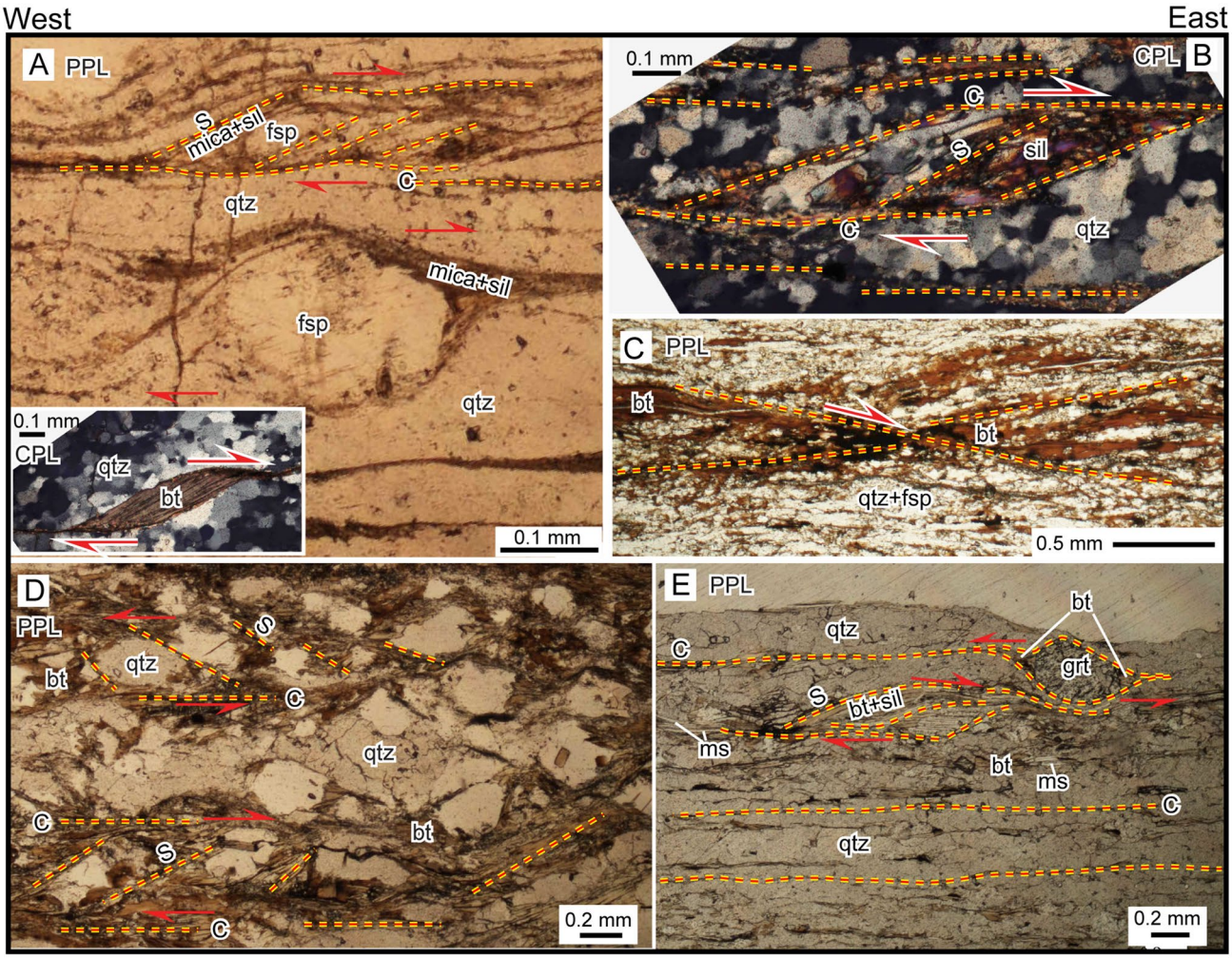

Fig. 8 Thin-section kinematic indicators on the plane perpendicular to the foliation and parallel to the lineation (the right side of each photo points to the east). **A**–**C** S-C structures of synkinematic sillimanite, delta-porphyroclast, mica fish, and shear band showing top-to-ESE shear. **D**–**E** S-C structures and sigma-porphyroclasts showing top-to-WNW shear and coexistence of top-to-ESE and top-to-WNW shear in the microscale. *bt* biotite, *fsp* feldspar, *grt* garnet, *ms* muscovite, *qtz* quartz, *sil* sillimanite, *PPL* plane polarized light, *CPL* cross polarized light

(MCH-1) from the roof shear zone of the SNC is a garnet-muscovite-biotite quartzofeldspathic mylonite containing minor muscovite quartzofeldspathic melt (Fig. 11A-i). The latter occurs as ~ 1 to 25 cm thick synkinematic melt patches and 1−10 cm thick layers, forming S-C structures and/or sigma-type asymmetric kinematic indicators indicative of top-to-ESE shear. Biotites from the mylonitic gneiss (Fig. 11A-ii) and muscovites from the synkinematic melt (Fig. 11A-iii) were picked for $^{40}Ar/^{39}Ar$ analysis. The sample (MCH-23) from the interior of the Upper SNC is a thin (1−5 cm), coarse-grained, synkinematic felsic melt that is composed of garnet, tourmaline, muscovite, potassium-feldspar, plagioclase, and quartz along with minor biotite and sillimanite (Fig. 11B-i). Some muscovites were variably strained and some potassium-feldspar was partially replaced along grain boundaries by myrmekite (Fig. 11B-ii, -iii); such grains were avoided during picking.

Rocks were crushed, sieved, washed, and hand-picked for pure biotite, muscovite, and feldspar mineral separates before being analyzed at the Geochronology laboratory at the University of Alaska, Fairbanks. Samples and standards were irradiated in the McMaster Nuclear Reactor at McMaster University in Hamilton, Ontario, Canada. The mineral MMhb-1 (Samson and Alexander 1987) with an age of 523.5 Ma (Renne et al. 1994) was used to monitor neutron flux. The monitor minerals and unknown samples were heated in an ultra-high vacuum extraction line using a 6-W argon-ion laser following the technique described in York et al. (1981) and Benowitz et al. (2014). Samples

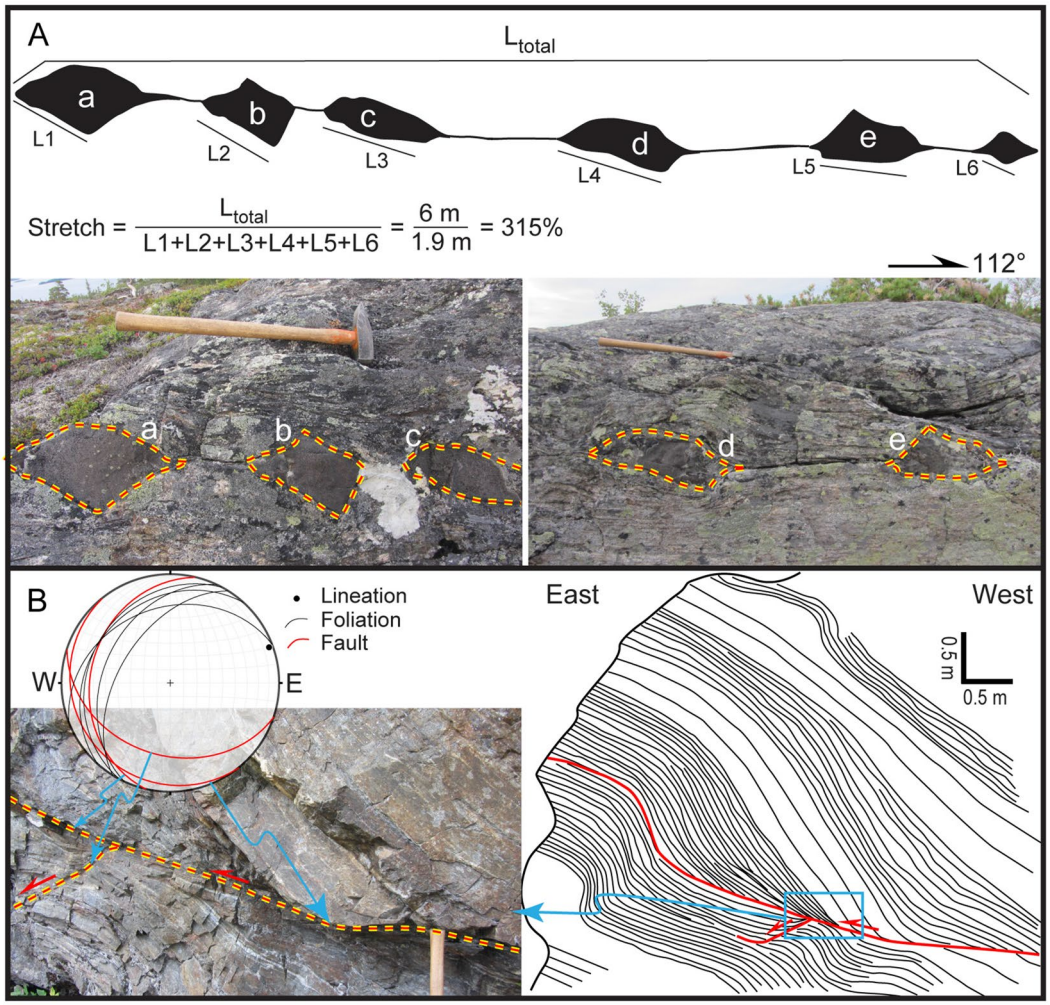

Fig. 9 **A** Boudinaged mafic dyke along the lineation providing an estimate of the minimum amount of stretch (about 315%). **B** Top-to-ESE thrust that is partly oblique and partly parallel to the foliation at the base of the Middle Seve Nappe Complex in the eastern area, Fig. 2B

were analyzed in a VG-3600 mass spectrometer at the Geophysical Institute, University of Alaska, Fairbanks. The argon isotopes measured were corrected for system blank and mass discrimination, as well as calcium, potassium and chlorine interference reactions following procedures outlined in McDougall and Harrison (1999). Correction factors for nucleogenic interferences during irradiation were determined from irradiated CaF_2 and K_2SO_4. Mass discrimination was monitored by running calibrated air shots. The mass discrimination during these experiments was 1.3% per mass unit. While doing our experiments, calibration measurements were made on a weekly to monthly basis to check for changes in mass discrimination with no significant variation seen during these intervals. Each of the mica separates has been heated in eight steps and the potassium-feldspar in eleven steps.

A summary of the multi-grain step-heating $^{40}Ar/^{39}Ar$ results and age spectra are given in Fig. 11C, with all ages quoted to the ± 1 sigma level and calculated using the constants of Renne et al. (2010). The spectrum provides a plateau age if three or more consecutive gas fractions represent at least 50% of the total gas released and are within two standard deviations of each other (Mean Square Weighted Deviation ≤ 2.5). Otherwise, an integrated age is calculated for those consecutive steps and is based on weighted average of the data with error at the 95% confidence level. The complete step-heating data are tabulated in Table S1.

Results

The $^{40}Ar/^{39}Ar$ data of the muscovite and biotite separates are characterized by flat age spectra showing no signs of argon loss (Fig. 11C). For the MCH-1 muscovite, 99.3% of ^{39}Ar was released in the last two of the eight steps during the heating experiment. These two steps give concordant ages within 1σ error and yield an integrated age of

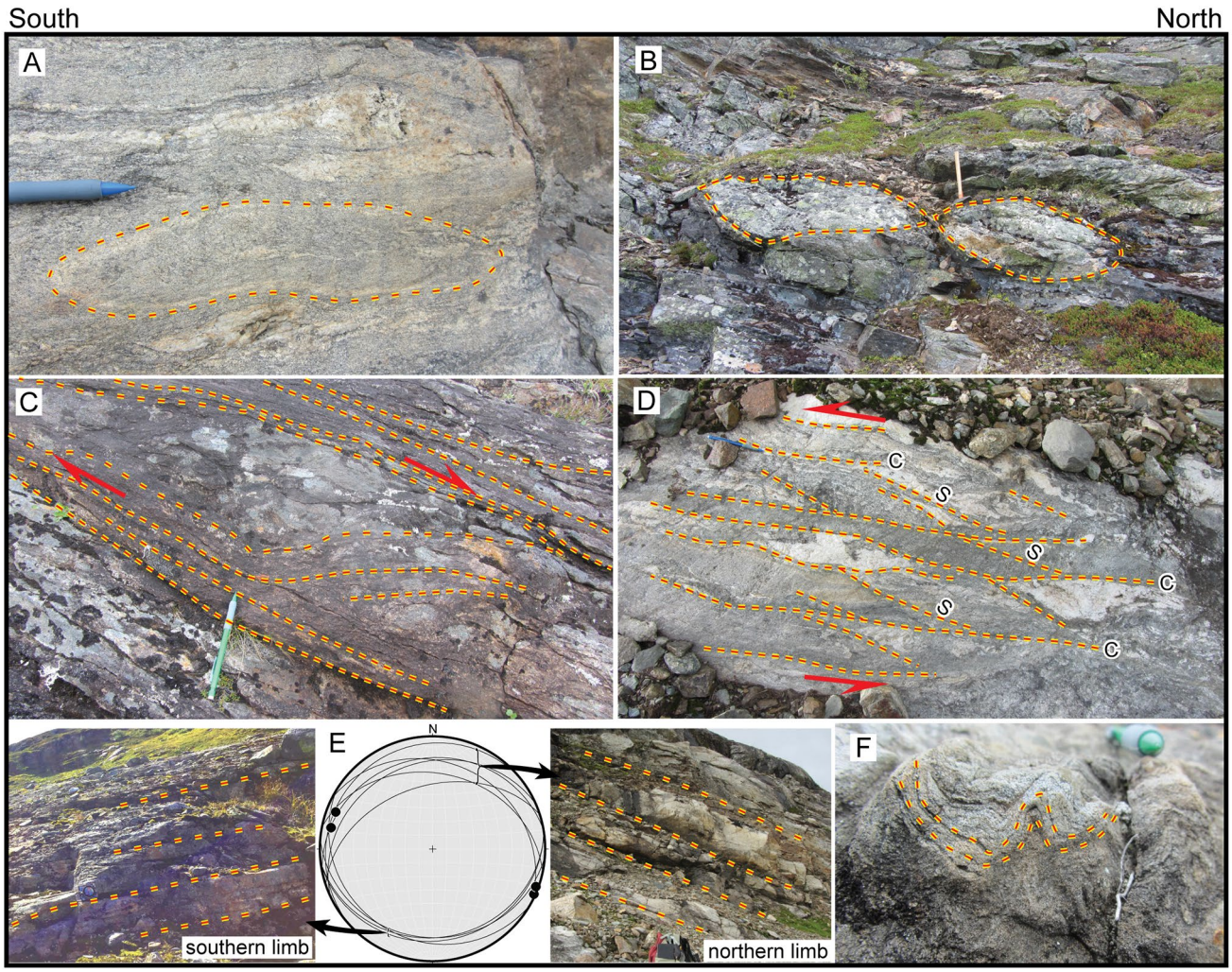

Fig. 10 Outcrop structures on lineation-normal planes in the Seve Nappe Complex (SNC), looking WNW. **A** Flattened sheath folds. **B** Boudinaged felsic melt with a symmetric geometry. **C** Asymmetric blocks of quartzofeldspathic gneiss in the Middle SNC showing a top-to-NNE (to the right in the photograph) non-coaxial shear. **D** S-C structures of quartzofeldspathic gneiss in the bottom of the Middle SNC showing a top-to-SSW (to the left in the photograph) non-coaxial shear. **E** 100 s m-scale gentle folds, stereoplot showing gneissic foliation (line) and lineation (dot). **F** Centimeter-scale folds

418.1 ± 1.7 Ma, statistically indistinguishable from the total gas age of 418.8 ± 1.8 Ma (Fig. 11C-i). The MCH-1 biotite progressively released ^{39}Ar after the first step of the heating experiment. The seven steps (including 99.0% of ^{39}Ar released) give concordant ages within 1σ error and yield a plateau age of 415.7 ± 1.4 Ma, nearly identical with the total gas age of 415.6 ± 1.4 Ma (Fig. 11C-ii). The MCH-23 muscovite also released ^{39}Ar progressively after the second step with concordant ages within 1σ error. The six steps of 99.4% of ^{39}Ar released give a plateau age of 416.7 ± 1.4 Ma, identical to the total gas age of 416.7 ± 1.4 Ma (Fig. 11C-iii).

The potassium-feldspar from sample MCH-23 gave a staircase age-spectrum (Fig. 11C-iv). After the first three steps, a total amount of 98.6% ^{39}Ar was progressively released in eight steps. The ^{40}Ar/^{39}Ar ratio steadily increases during heating and the individual steps yield apparent ^{40}Ar/^{39}Ar ages ranging from ~ 340 to ~ 400 Ma. Three continuous steps (gray boxes in Fig. 11C-iv) including 23.5% ^{39}Ar released are concordant within 1σ error and yield an integrated age of 390.0 ± 2.0 Ma. The minimum age of ~ 340 Ma is defined by the fourth step including 25.1% ^{39}Ar released.

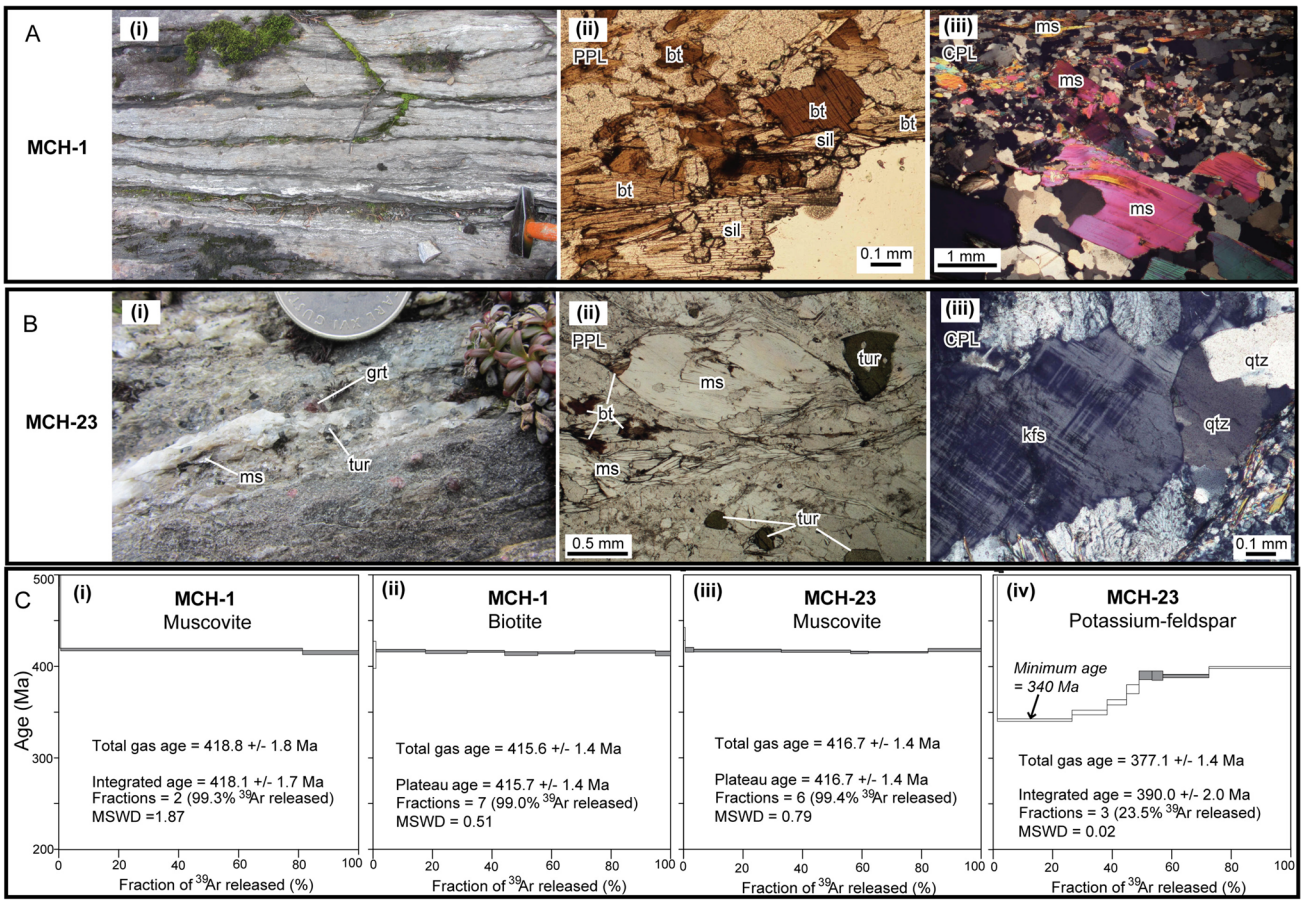

Fig. 11 Outcrops, thin-sections, and $^{40}Ar/^{39}Ar$ age spectra (1σ errors) of samples MCH-1 and MCH-23. The gray boxes in the age spectra indicate the steps used for calculation of integrated or plateau ages. *bt* biotite, *grt* garnet, *kfs* potassium-feldspar, *ms* muscovite, qtz quartz, *sil* sillimanite, *tur* tourmaline, *PPL* plane polarized light, *CPL* cross polarized light

Discussion

Exhumation of the central Jämtland Seve Nappe Complex following migmatization and prior to extensional collapse

Exhumation of the central Jämtland SNC from (U)HP conditions to crustal levels where migmatites formed could be generally defined by the P–T–t data published by previous works. The extensional collapse of the Scandinavian Caledonides is understood as a part of the Devonian orogen-scale, hinterland-directed normal-faulting that likely started between ~ 408 and ~ 402 Ma in southern Norway (Fossen and Dunlap 1998; Fossen 2010). The new data reported in the current study aim to constrain the exhumation of the central Jämtland SNC between these two periods, i.e., exhumation from crustal levels where migmatites formed to crustal levels where extensional faulting takes over the deformation.

Nature of deformation during the exhumation

The post-migmatization ductile shear fabrics of the Upper and Middle SNC mapped in this study are (1) structurally concordant without overprinting and/or crosscutting relationships, (2) broadly similar in metamorphic grade, (3) related to the foreland-directed transport of the SNC, and (4) are cut by several normal faults or extensional shear zones (Sjöström et al. 1996). Therefore, the ductile shear fabrics of the Upper–Middle SNC are broadly coeval and likely record the bulk deformation path after the migmatization of the SNC and prior to the extensional collapse of the orogen.

The maximum principal strain axis, *X*, parallel to the *X*-axis of the finite strain ellipsoid, is revealed by the dominant ductile ridge-in-groove lineations. The lineations generally trend ESE-WNW and plunge shallowly (< 20°) to subhorizontally (Figs. 2A and 6). Structures formed along this direction are asymmetric on the plane perpendicular to the foliation and parallel to the lineation (e.g., sigma- and delta-porphyroclasts, S-C structures, mica fish, shear bands,

asymmetric folds, Figs. 7 and 8), which indicates that the general strain component along the *X*-axis can be described as a non-coaxial shear path. Migmatites and migmatitic gneisses are locally preserved between shear zones in the Middle SNC (e.g., the outcrop in Fig. 12), which suggests that the *X*-axis strain was partitioned.

The minimum principal strain axis, *Z*, is constrained to be subvertical on the basis of boudinage structures such as the boudinaged mafic dyke exposed on the plane perpendicular to the foliation and parallel to the lineation (Fig. 9A), as well as the boudinaged quartzofeldspathic layer exposed on the plane perpendicular to the lineation (Fig. 10B). The flattened sheath folds on the lineation-normal plane (Fig. 10A) also support a subvertical shortening along the *Z*-axis. These structures show that the general strain component along the *Z*-axis was characteristic of vertical flattening.

The strain component along the intermediate principal strain axis, *Y*, is revealed by structures exposed on the lineation-normal plane. The asymmetric blocks (Fig. 10C), shear bands, and S-C structures (Fig. 10D) found on this plane show lateral flow of ductile rocks along the foliation, top-to-NNE at the top and top-to-SSW at the bottom of the Middle SNC. This suggests that the general strain component perpendicular to the lineation and parallel to the foliation could be described as a non-coaxial shear path. The various scales of folds on the lineation-normal plane with axial surfaces parallel to the lineation (Fig. 10E,F) might indicate local convergent flow of ductile rocks along ESE-WNW. An alternative interpretation, especially for the 100 s m-scale gentle folds (Fig. 10E), is that the variation of thickness of the underlying rocks caused perturbation of the overlying ductile flow.

In summary, the bulk deformation path of the Upper–Middle SNC in central Jämtland is consistent with a triclinic or general shear (Jiang and Williams 1998; Lin et al. 1998; 2007), which is defined by a dominant non-coaxial shear along ESE-WNW, a subordinate non-coaxial shear along NNE-SSW, and a vertical flattening component (Fig. 12). Because the microstructures of quartz and feldspar (Fig. 5) and formation of stable garnet/amphibole and syn-kinematic sillimanite (e.g., Fig. 8B) indicate relatively high temperatures during the ductile shear, this deformation path describes the nature of the ductile flow due to the exhumation of the SNC through mid-crustal levels. This is supported

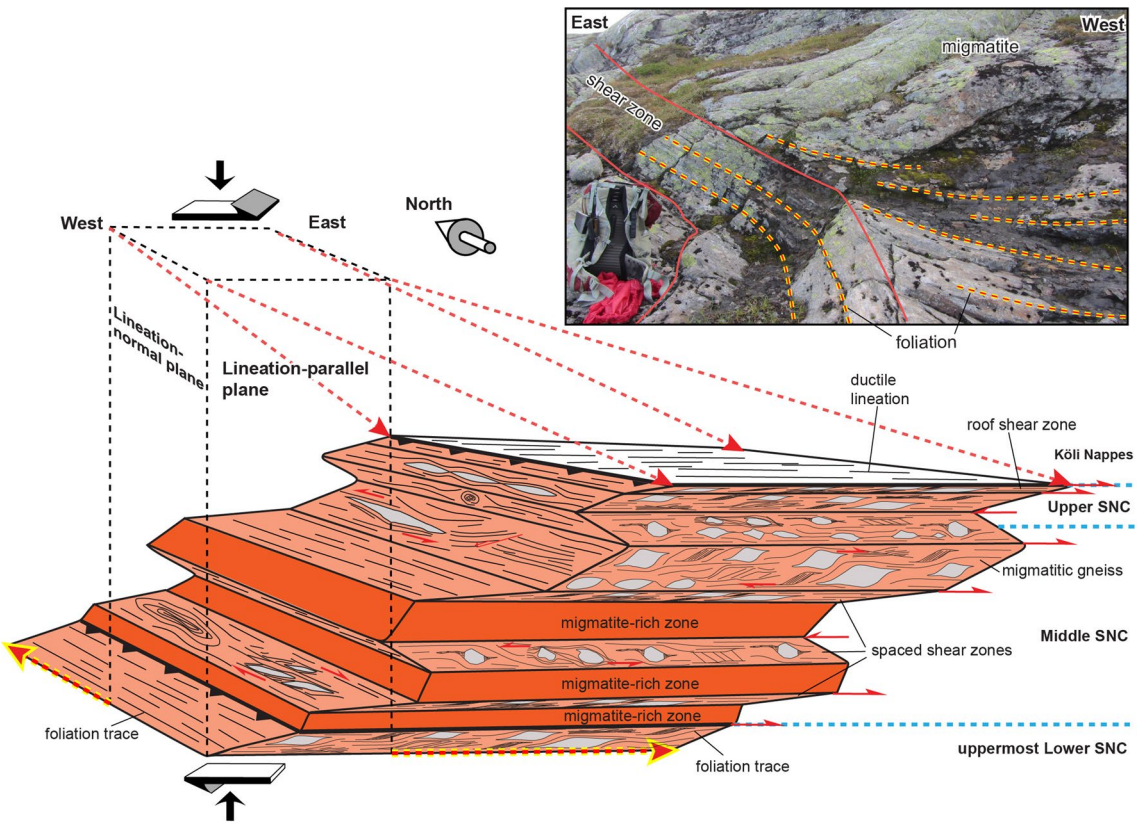

Fig. 12 Three-dimensional diagram summarizing the structures and kinematics of the post-migmatization ductile deformation of the Seve Nappe Complex (SNC) in the study area. Note the opposite senses of non-coaxial shear on the lineation-parallel plane and secondary non-coaxial shear on the lineation-normal plane. See Figs. 7 and 8 for examples of structures on the lineation-parallel plane and Fig. 10 for those on the lineation-normal plane. The picture shows one of the internal shear zones in the Middle SNC

by the P–T conditions of 0.8−1 GPa and ~ 600 to 650 °C for the formation of mylonitic fabrics of the lower SNC in the COSC-1 borehole (Fig. 1B, Giuntoli et al. 2018, 2020). Previous studies have described this deformation as a non-coaxial progressive flow to the east or southeast combined with concurrent vertical ductile thinning (Bergman and Sjöstrom 1997; Bender et al. 2018). The current study supports these conclusions and provides additional constraints on the deformation, which are: (1) the bulk deformation path is triclinic; (2) the dominant top-to-ESE non-coaxial shear along the foliation had various flow rates at different structural levels. The second constraint is based on the kinematically contrasted shear zones of various scales at different structural levels (Fig. 2A), i.e., structurally concordant, top-to-ESE and top-to-WNW shear fabrics from the Upper SNC to the Middle SNC (Figs. 7, 8).

Timing of exhumation and cooling

Stable amphibole/garnet and newly formed sillimanite in mylonite, and relatively high temperature microstructures including grain boundary migration recrystallization of quartz (Fig. 5A,C), grain boundary area reduction of quartz (Fig. 5B), and ductile deformation of plagioclase (Fig. 5D) jointly indicate that the deformation in the shear zones of the Upper and Middle SNC occurred at temperatures (likely > 500 °C, Passchier and Trouw 2005) higher than the argon closure temperature intervals of muscovite (~ 450 to 350 °C), biotite (~ 380 to 300 °C), and potassium-feldspar (~ 350 to 150 °C) in crustal rocks (e.g., McDougall and Harrison 1999; Foster et al. 2010). This interpretation is consistent with the amphibolite-facies metamorphism recorded by parageneses in the mylonitic Upper SNC (Sjöström 1984). The muscovite and biotite ages of sample MCH-1 (418.1 ± 1.7 Ma, 415.7 ± 1.4 Ma, Fig. 11C-i, -ii, respectively) and the muscovite age of sample MCH-23 (416.7 ± 1.4 Ma, Fig. 11C-iii), therefore, are interpreted to reflect the timing of mica cooling in the Upper SNC through temperatures of ~ 450 to 300 °C. The $^{40}Ar/^{39}Ar$ age spectrum of the potassium-feldspar from sample MCH-23 reveal further cooling of the Upper SNC possibly through temperatures of ~ 180 to 150 °C by 340 Ma (the minimum age in Fig. 11C-iv). These cooling data indicate that the argon isotopic systems in micas and potassium-feldspar were not disrupted after 418−416 Ma and 340 Ma, respectively. This suggests that there was no pervasive deformation or significant thermal event in the SNC following 416 Ma, which is supported by the metamorphic patterns of rocks from either side of the Seve−Köli boundary indicating no post-metamorphic movements (Bergman 1992).

In conjunction with the Llandovery turbidites and conglomerates of the Änge group underlying the Middle allochthons in central Jämtland (Kulling 1933), the timing of exhumation of the SNC following the migmatization is bracketed between 433 and 418 Ma. This timing is well supported by recent geochronology data from the SNC, including the multi-mineral Rb–Sr isochron ages of mylonitic rocks from outcrops across the SNC in central Jämtland (433–423 Ma) (Bender et al. 2019) and the Lower SNC in the COSC-1 borehole (~ 429 Ma) (Fig. 1B, Glodny et al. 2017), the Th-U–Pb ages (424 ± 6, 423 ± 13 Ma) of fluid-assisted grown monazites in the Middle SNC at Åreskutan (Majka et al. 2012), the U–Pb ages of 439 ± 4 Ma of zircon overgrowths from the diamond-bearing gneiss at Tväråklumparna (Walczak et al. 2022), and the U–Pb ages of synkinematic titanite (429 ± 20 Ma, 417 ± 9 Ma) in the Lower SNC mylonite of the COSC-1 borehole (Giuntoli et al. 2020). Thereafter, the SNC underwent cooling through ~ 450 to 300 °C at about 418−416 Ma and ~ 180 to 150 °C possibly at about 340 Ma without any pervasive deformation, except for extensional collapse along several normal fault zones (e.g., Sjöström et al. 1996).

Exhumation of the central Jämtland Seve Nappe Complex from mantle depths beneath the hinterland to the Earth's surface in the foreland

The regional geology and published P–T–t data of the central Jämtland SNC along with the new structure and $^{40}Ar/^{39}Ar$ data of the current study provide insights into a complete view of the exhumation of the SNC. The following discussion aims to constrain the exhumation of the central Jämtland SNC from depths of (U)HP conditions beneath the hinterland to the Earth's surface above the foreland basin. The total exhumation of the central Jämtland SNC includes > 100 km vertical and > 350 km horizontal displacements. With the hyperextension model of the Baltica margin (e.g., Andersen et al. 2012, 2022; Jakob et al. 2019), the horizontal displacement of the SNC would be > 1200 km. The data defining the exhumation of the SNC are summarized in Fig. 13 and the geologic context of the central Scandinavian Caledonides for each stage of the exhumation is shown in Fig. 14.

A variety of mechanisms have been proposed for exhuming rocks from mantle and crustal depths, such as subduction channel flow (e.g., Gerya et al. 2002), thrusting of crustal slivers (Chemenda et al. 1995), extrusion (e.g., Thompson et al. 1997; Ring and Glodny 2010), buoyancy (e.g., Warren 2013), eduction (i.e., reversal of subduction, Andersen et al. 1991), piggyback translation (Brueckner and Cuthbert 2013), tectonic under-pressure by delamination, slab rollback, or microplate rotation (e.g., Hacker and Gerya 2013; Majka et al. 2014b), trans-mantle diapirs (e.g., Hacker and Gerya 2013), surface processes, and extensional detachment faulting (e.g., Ma et al. 2019, 2021). Exhumation of HP/

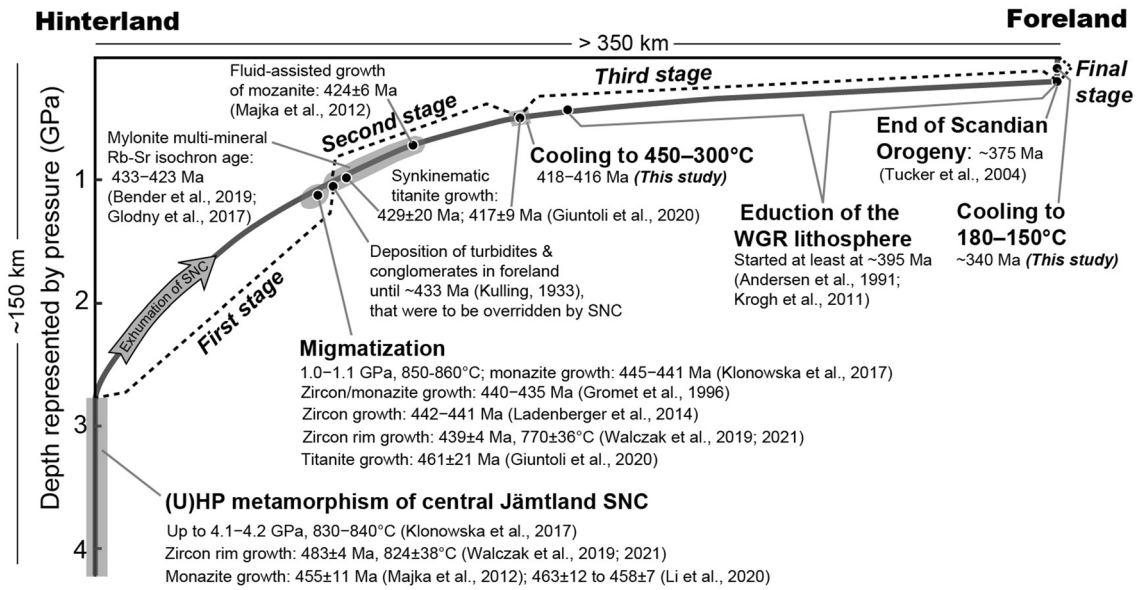

Fig. 13 Summary of the P–T–t data and sources defining the four stages exhumation of the Seve Nappe Complex in central Jämtland along a schematic exhumation trajectory from mantle depths beneath the hinterland to the Earth's surface in the foreland. *WGR* Western Gneiss Region

UHP rocks can be generally described as a fast process controlled by density contrast followed by a slow process that is generally influenced by tectonic and surface processes (e.g., Yamato et al. 2008). Exhumation of the SNC from (U)HP conditions to crustal levels where migmatites formed was likely rapid such that some of the HP/UHP mineral assemblages can survive from decompressional melting (e.g., Thompson et al. 1997; Yamato et al. 2008) and form the eclogite, garnet pyroxenite, garnet peridotite, and diamond-bearing gneiss currently preserved in the SNC. Prior to the subduction of the central Jämtland SNC (Fig. 14A), its protoliths occurred as passive margin sequences overlying the westernmost Baltica and intruded by mafic dykes. During the Ordovician, the SNC and the underlying continental lithosphere were probably subducted to UHP and HP conditions (Fig. 14B) under an oceanic terrane represented by the Lower Köli Nappes.

The depths from which the central Jämtland SNC was exhumed are constrained by P–T conditions of peak metamorphism (4.1–4.2 GPa and 830–840 °C) based on garnet + phengite + kyanite + rutile assemblages of paragneisses from Åreskutan (Fig. 1B), which was verified by the identification of diamond inclusions in garnet of the same rocks (Klonowska et al. 2017). About 10 km to the west of the study area at Tväråklumparna (Fig. 1C), metamorphic diamonds were also discovered as inclusions in garnet (Majka et al. 2014b). Zircon overgrowth and monazite from these diamond-bearing gneisses have been dated and provide records of UHP and HP metamorphism at 483 ± 4 Ma (Walczak et al. 2022) and 455 ± 11 Ma (Majka et al. 2012), respectively. The SNC of the current study, located between these diamond-discovery sites and exposing the same tectonostratigraphic units, most likely underwent a similar metamorphism P–T–t trajectory. Two features in support for this interpretation are (1) the occurrence of radial fractures in garnet around quartz inclusions (Fig. 3F) suggesting transformation of former coesite, and (2) the dark-rose garnets (grt I in Fig. 3C) in equilibrium with kyanite (Fig. 3C,D) where the former probably correspond to the Ca- and Mg-rich garnets formed at UHP conditions in the Middle SNC of Åreskutan (Klonowska et al. 2017).

First stage exhumation: upward flow from UHP depths due to buoyancy

On the basis of literature data, it is inferred that the first stage exhumation of the central Jämtland SNC was initiated following the HP metamorphism, possibly at or slightly after 455 Ma. The first stage exhumation was likely characterized by a nearly isothermal decompression of the SNC rocks from depths of (U)HP conditions (≥ 100 km, Klonowska et al. 2017) to depths of granulite-facies (≈ 40 km for a granitic composition of the overlying continental crust) in ~ 455 to 433 Ma (Figs. 14, 15C).

The exhumation of the UHP rocks during the decompression was probably dominantly driven by buoyancy, because at temperatures of 800–900 °C, a quartzofeldspathic continental crust with minor mafic/ultramafic rocks, such as the SNC, would be positively buoyant to the mantle (Hacker and Gerya 2013). In general, mechanisms that could exhume

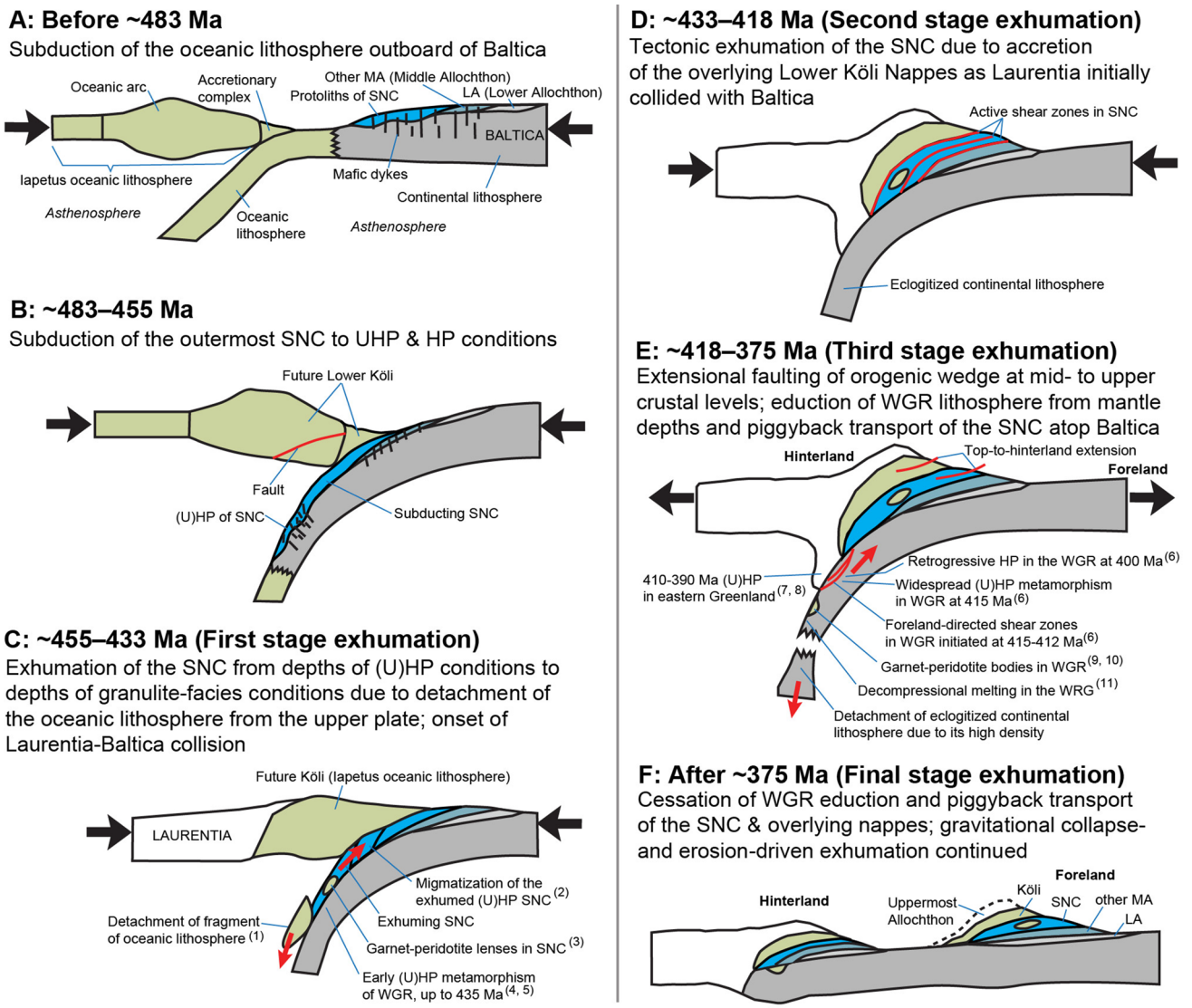

Fig. 14 Subduction and exhumation of the Seve Nappe Complex (SNC) in the geologic context of central Scandinavian Caledonides. Data sources: (1) Majka et al. (2014b), (2) Ladenberger et al. (2014), (3) Brueckner et al. (2004), (4) Beckman et al. (2014), (5) Spengler et al. (2009), (6) Young (2017), (7) Gilotti et al. (2008), (8) Augland et al. (2010), (9) Cuthbert et al. (2000), (10) Brueckner et al. (2010), (11) Krogh et al. (2011). *WGR* Western Gneiss Region

rocks for > 100 km vertically would be likely controlled by (1) *positive buoyancy* of the exhuming rocks, (2) *availability of space* for storing the exhumed rocks at shallower depths and for accommodating the increased volume of the partially melted exhuming rocks during isothermal decompression, and (3) *local tectonic forces* to trigger the upward flow of the exhuming rocks (e.g., Warren 2013). To promote the exhumation of the SNC, detachment of a lithospheric mantle fragment above the subduction zone, as proposed by Majka et al. (2014b), would provide both a local tectonic force (i.e., tectonic under-pressure, Majka et al. 2014b) and space at shallower depths (Fig. 14C). The rupture of this mantle fragment probably resulted from contractional stresses during the arc-continent convergence (Fig. 14B) that resulted in the deposition of the mid-Ordovician turbidites in the foreland basin (Gee et al. 2014). Alternatively, progressive hydration of the hanging-wall mantle wedge could widen the subduction channel and trigger the onset of forced return flow for exhuming UHP rocks (Gerya et al. 2002). However, there is no evidence for such hydrated mantle rocks in the central Jämtland SNC. The fabrics of the blocks enclosed in the migmatitic gneisses (Fig. 4C,D, and S1-B-o) were potentially developed during this period of the exhumation. Positive buoyancy of the bulk SNC rocks probably played an important role in this stage (Warren 2013). Near the end of the first stage exhumation (Fig. 14C), UHP metamorphism

was recorded in the Western Gneiss Region (WGR) beneath the hinterland by the 434 ± 3 Ma Flemsøy peridotite (Spengler et al. 2009).

Second stage exhumation: tectonic flow at crustal levels resulted from accretion of the Lower Köli Nappes

The second stage exhumation of the central Jämtland SNC started at depths corresponding to 1.0–1.1 GPa and 850–860 °C following the migmatization at 440–435 Ma (Fig. 13). Since the SNC underwent decompression melting during the first stage exhumation, the density contrast between the SNC and surrounding crust during the second stage exhumation was probably minimal. Therefore, the exhumation of the SNC thereafter was likely not controlled by buoyancy.

The second stage exhumation was characterized by ductile shear of the migmatized SNC, likely associated with foreland-directed thrusting of the Lower Köli Nappes (discussed below) during 433−418 Ma (Fig. 14D). Based on variations of metamorphic grade, this stage of the exhumation of the SNC in lower granulite- to amphibolite-facies conditions was spatially confined between the underlying Särv Nappes and the overlying Köli Nappes. This is demonstrated by an upwards increase in metamorphic grade of the greenschist-facies Särv Nappes to garnet-mica schists and amphibolites, and a local downwards increase in grade of the Köli Nappes deviating from the general greenschist- to lower amphibolite-facies, reflecting downwards and upwards heat fluxes, respectively, from the intervening SNC (Sjöström 1984; Bergman 1992; Bergman and Sjöström 1997).

The structures and kinematics of the ductile deformation revealed in the current study (Fig. 12) provide key insights into the mechanism of the second stage exhumation. The evidence for top-to-WNW shear (Figs. 7H, I, 8D–F) that was concordant with the dominant top-to-ESE shear is important because coexistence of opposite kinematics across different structural levels indicates various rates of ductile flow extruding toward the foreland. Therefore, extrusion tectonics (e.g., Thompson et al. 1997), should have contributed to the exhumation of the SNC at certain structural levels in addition to the dominant foreland-directed non-coaxial shear (Fig. 12). This interpretation is consistent with the spatial relationship that the SNC was confined by the Särv and Köli Nappes, which provides proper boundary conditions for extruding. An extrusion wedge bounded by a normal fault (top-to-NW) at the top and a coeval thrust (top-to-SE) at the base (e.g., Ring and Glodny 2010) was proposed for the exhumation of the entire Upper and Middle SNC in the area at the Västerbotten-Jämtland border (Fig. 1A) (Grimmer et al. 2015). A key premise for this model was the top-to-NW slip along the roof shear zone. The kinematics of the roof shear zone in the current study, however, is dominated by top-to-ESE shear. An extrusion wedge as a solitary mechanism for exhuming the whole Upper and Middle SNC (Ring and Glodny 2010), therefore, is not tenable for the SNC in central Jämtland. Bender et al. (2018) also showed that evidence for extrusion of the entire SNC is lacking in Jämtland. The extensive top-to-ESE slip suggests that the non-coaxial shear of the SNC had a gradient of displacement that progressively decreased toward lower structural levels. Rocks at the top of the SNC, therefore, should record the largest ESE-ward displacement. The mylonitic−ultramylonitic fabrics of the roof shear zone containing the highest degree of strain support this interpretation. This gradient of ductile flow could be interpreted by two alternative processes: (1) the overriding Lower Köli Nappes were thrusting toward the ESE, which induced passive flow of the underlying SNC rocks; or (2) the SNC was extruding toward the ESE with highest flow rates at the top and progressively decreased rates toward lower structural levels. The latter process is not common because the highest rate of particle movement during extrusion is expected to be in the middle of the extrusion channel (Thompson et al. 1997). We, therefore, consider that the ESE-ward thrusting of the overlying Lower Köli Nappes due to the initial collision between Laurentia and Baltica since ~ 440 Ma (Spengler et al. 2009) was the primary cause for the non-coaxial flow of the central Jämtland SNC. Extrusion likely contributed subordinately at some structural levels for exhuming the SNC as shown by the sparse outcrops displaying opposite sense of shearing. The extrusion was probably later given to thrusting due to cooling of the SNC (e.g., Gee et al. 2013). This interpretation requires that at least the lowermost Köli Nappes had been emplaced upon the central Jämtland SNC prior to or during the second stage exhumation of the SNC, which is supported by the following evidence from the Köli-Seve boundary.

Peak metamorphism during thrusting of the Lower Köli Nappes in central Jämtland is indicated by the shared amphibolite-facies mylonites along the basal shear zone of the Köli Nappes and the roof shear zone of the SNC (Bergman 1992). Also, P–T paths demonstrate metamorphic convergence across the boundary between the Lower Köli Nappes and the Upper SNC (Bergman 1992). The accretion of the Lower Köli Nappes onto the SNC, therefore, should be broadly coeval with the second stage exhumation of the SNC.

Third stage exhumation: piggy-back transport due to eduction of the Western Gneiss Region lithosphere

The third stage exhumation of the central Jämtland SNC (Fig. 14E) was likely expediated by eduction of the WGR lithosphere (Fig. 1B) beneath the hinterland (Andersen et al. 1991). The WGR locally underwent decompressional melting at about 395 Ma (Fig. 14E) (Krogh et al. 2011), which followed the widespread (U)HP metamorphism in

the WGR in 415−400 Ma (Kylander-Clark et al. 2007; Krogh et al. 2011) and initiation of foreland-directed eclogite-facies shear zones in 415−412 Ma (Young 2017). The decompressional melting was likely caused by eduction of the Baltica lithosphere possibly triggered by detaching of the eclogitized continental lithosphere outboard of the WGR. Available muscovite cooling ages of the SNC and Köli Nappes in central Jämtland vary between 425–410 Ma (Fig. 1B) (Dallmeyer et al. 1985), similar to those in the eastern Trondheim Nappe Complex (Fig. 1B). This suggests that, prior to ~ 410 Ma, the Upper and Middle Allochthons in these regions were tectonically active and cooled through argon closure in muscovite diachronously at different structural levels and locations. To the west, after ~ 410 Ma, the western Trondheim Nappe Complex and WGR cooled through argon closure in muscovite systematically, i.e., progressively younging westward until ~ 380 Ma along the Norwegian west coast (Fig. 1B) (Walsh et al. 2013). This systematic, post-410 Ma cooling is one of the key pieces of evidence supporting eduction of a coherent slab as the main mechanism for exhuming the (U)HP WGR (Andersen et al. 1991; Young et al. 2007). Other evidence such as westward decrease in titanite ages and increase in regional pressure gradient, and E-W exhumational fabrics are discussed by earlier studies (e.g., Young et al. 2007; Kylander-Clark et al. 2008; Hacker et al. 2010; Spencer et al. 2013). Therefore, the third stage exhumation of the central Jämtland SNC was likely characterized by piggyback transport of the SNC and the surrounding nappes atop Baltica toward the foreland (Brueckner and Cuthbert 2013). $^{40}Ar/^{39}Ar$ isotopes of mica and potassium-feldspar could record the cooling ages during this stage because it is expected no significant deformation to reset the $^{40}Ar/^{39}Ar$ system with the piggyback model (Brueckner and Cuthbert 2013). The mica cooling ages of 418–416 Ma obtained from the SNC roof shear zone in the current study are interpreted to document cooling through 450–300 °C at the early phase of the third stage exhumation. The top-to-W and top-to-E extensional shear zones truncating the tectonostratigraphy with displacements on the order of a few kilometers or tens of kilometers along some of the larger zones in the WGR (e.g., Fossen and Dunlap 1998) and in central Jämtland (e.g., Sjöström et al. 1996; Sjöstrand 1999) likely formed in this time at mid- to upper-crustal levels, which contributed to vertical thinning of the allochthon pile and additional exhumation of the SNC.

At the Laurentian side, (U)HP rocks of 410−390 Ma now exposed in eastern Greenland (Gilotti et al. 2008; Augland et al. 2010) might be exhumed during this stage as the WGR was being educted. The ending of the third stage and beginning of the fourth stage exhumation of the SNC (Fig. 13) is marked by the completion of the Scandian Orogeny at ~ 375 Ma in the central Scandinavian Caledonides (Tucker et al. 2004). The eduction of the WGR lithosphere probably was the major contributor for the > 350 km horizontal transport of the central Jämtland SNC into the cratonic interior without pervasive deformation (Brueckner and Cuthbert 2013).

Final stage exhumation: uplift due to gravitational collapse and erosion

The final stage exhumation of the central Jämtland SNC was likely driven by gravitational collapse and surface processes (Fig. 14F), as the Scandian contractional tectonics ceased at ~ 375 Ma (Tucker et al. 2004). The $^{40}Ar/^{39}Ar$ data of potassium-feldspar (Fig. 11C-iv) in the current study appear to have captured a moment of cooling through ~ 180 to 150 °C at about 340 Ma during this stage. Eventually, surface processes became the dominant mechanism for exhuming the SNC until it was exposed at the Earth's surface.

Concluding remarks

This study integrates newly acquired structure and $^{40}Ar/^{39}Ar$ data from the central Jämtland SNC into the published P–T–t dataset and regional geology, which forms the framework of our understanding of the exhumation of the central Jämtland SNC from (U)HP depths beneath the Caledonian hinterland to the Earth's surface in the foreland. The following summarizes the main conclusions.

1. Structural data from the post-migmatization, pre-normal-faulting fabrics of the central Jämtland SNC demonstrates that the bulk deformation was triclinic, which is defined by a predominantly top-to-ESE non-coaxial shear along subhorizontal foliations, a subordinate non-coaxial shear along the foliation and orthogonal to the WNW-ESE lineation, and a subvertical flattening component (Fig. 12). An extrusion component is also documented at several structural levels. This deformation is characteristic of the second stage exhumation of the central Jämtland SNC.
2. $^{40}Ar/^{39}Ar$ data from the SNC roof shear zone and the Upper SNC reveal cooling through ~ 450 to 300 °C at about 418−416 Ma and through ~ 180 to 150 °C at about 340 Ma (Fig. 11). These data indicate that the second stage exhumation occurred prior to ~ 418 Ma and provide insights into the cooling history of the third and final stages exhumation of the central Jämtland SNC.
3. In combination with published P–T–t data, four stages of exhumation (Fig. 13) of the central Jämtland SNC are summarized: (1) buoyancy-driven exhumation triggered by tectonic under-pressure, characterized by isothermal decompression and upward flow of the SNC from (U)HP depths to granulite-facies depths (Fig. 14C); (2) tec-

tonic exhumation at crustal levels resulted from accretion of the Lower Köli Nappes, characterized by dominant foreland-directed thrusting, vertical thinning, and minor extrusion (Fig. 14D); (3) eduction of the WGR lithosphere at depths and extensional faulting at mid- to upper-crustal levels, largely characterized by > 350 km piggyback transport of the central Jämtland SNC from the hinterland to the foreland (from E to F in Fig. 14); and (4) gravitational collapse- and erosion-driven exhumation uplifting the SNC to the Earth's surface (after F in Fig. 14).

4. The first three stages of the exhumation involved simultaneous combination of vertical and horizontal displacements, i.e., toward the Earth's surface and the Caledonian foreland, respectively. The first stage was likely dominated by vertical movement while the third stage by horizontal movement. The latter probably made the greatest contribution to the > 350 km west-to-east transport of the central Jämtland SNC, which might be considered as a combination of relative displacements along fault zones at various levels above the Baltic basement and the absolute distance traveled by Baltica itself during the eduction of the WGR lithosphere.

This study provides insights into the general processes of exhumation of deeply subducted continental rocks in orogenic belts using the SNC in central Jämtland as an example. Future work of the SNC may reveal a more inclusive model incorporating (i) diachronous exhumation of the SNC along the Scandinavian Caledonides and (ii) progressive exhumation of the SNC from and to different depths *across* the orogen between the foreland and hinterland.

Supplementary Information The online version contains supplementary material available at https://doi.org/10.1007/s00531-022-02205-1.

Acknowledgements Andrew Kylander–Clark and an anonymous reviewer are thanked for their helpful reviews that improved the manuscript. The Department of Geosciences of Auburn University partially supported Ma's field work in Sweden. Attendants of the 2016 Transcand excursion/workshop are greatly thanked for extensive discussions on the Caledonian geology. This study was supported by the National Science Centre (Poland) project 2014/14/ST10/00321 to Majka and the basic research project 41888101 of the National Natural Science Foundation of China.

References

Albrecht LG (2000) Early structural and metamorphic evolution of the Scandinavian Caledonides: a study of the eclogite-bearing Seve Nappe Complex at the Arctic Circle [PhD Thesis]. Lund University, Lund, p 132

Andersen TB, Jamtveit B, Dewey JF, Swensson E (1991) Subduction and eduction of continental crust: major mechanisms during continent-continent collision and orogenic extensional collapse, a model based on the south Norwegian Caledonides. Terra Nova 3:303–310

Andersen TB, Corfu F, Labrousse L, Osmundsen PT (2012) Evidence for hyperextension along the pre-Caledonian margin of Baltica. J Geol Soc 169:601–612

Andersen TB, Jakob J, Kjøll HJ, Tegner C (2022) Vestiges of the pre-caledonian passive margin of Baltica in the Scandinavian Caledonides: overview, revisions and control on the structure of the Mountain Belt. Geosciences. https://doi.org/10.3390/geosciences12020057

Andersson B (2015) Age and metamorphic conditions of the Tjeliken garnet–phengite gneiss (Swedish Caledonides). Geol Geophys Environ 41(1):55–56

Andersson A, Dahlman B, Gee DG, Sven S (1985) The Scandinavian alum shales. Avhandlingar Och Uppsatser I A4, Sveriges Geologiska Undersökning, p 50

Andréasson PG (1994) The Baltoscandian margin in neoproterozoic-early palaeozoic times Some constraints on terrane derivation and accretion in the Arctic Scandinavian Caledonides. Tectonophysics 231(1):1–32

Andréasson PG, Gee D, Sukotji S (1985) Seve eclogites in the Norrbotten Caledonides, Sweden. In: Gee DG, Sturt BA (eds) The Caledonide Orogen-Scandinavia and related areas. Wiley, Chichester, pp 887–901

Andréasson PG, Svenningsen OM, Albrecht L (1998) Dawn of Phanerozoic orogeny in the North Atlantic tract; Evidence from the Seve-Kalak Superterrane, Scandinavian Caledonides. GFF 120(2):159–172

Arnbom J-O (1980) Metamorphism of the Seve Nappes at Åreskutan, Swedish Caledonides. Geologiska Föreningen i Stockholm Förhandlingar 102(4):359–371

Augland LE, Andresen A, Corfu F (2010) Age, structural setting, and exhumation of the Liverpool Land eclogite terrane, East Greenland Caledonides. Lithosphere 2(4):267–286

Barnes C, Majka J, Schneider D, Walczak K, Bukała M, Kośmińska K, Tokarski T, Karlsson A (2019) High-spatial resolution dating of monazite and zircon reveals the timing of subduction–exhumation of the Vaimok Lens in the Seve Nappe Complex (Scandinavian Caledonides). Contrib Mineral Petrol. https://doi.org/10.1007/s00410-018-1539-1

Be'eri-Shlevin Y, Gee D, Claesson S, Ladenberger A, Majka J, Kirkland C, Robinson P, Frei D (2011) Provenance of Neoproterozoic sediments in the Särv nappes (Middle Allochthon) of the Scandinavian Caledonides: LA-ICP-MS and SIMS U–Pb dating of detrital zircons. Precambr Res 187(1):181–200

Beckholmen M (1982) Mylonites and pseudotachylites associated with thrusting of the Köli Nappes, Tännforsfältet, central Swedish Caledonides. Geologiska Föreningen i Stockholm Förhandlingar 104(1):23–32

Beckman V, Möller C, Söderlund U, Corfu F, Pallon J, Chamberlain KR (2014) Metamorphic zircon formation at the transition from gabbro to eclogite in Trollheimen–Surnadalen, Norwegian Caledonides. In: Corfu F, Gasser D, Chew DM (eds) New perspectives on the caledonides of scandinavia and related areas. Geological Society, London, Special Publication 390, pp 403–424

Bender H, Ring U, Almqvist BSG, Grasemann B, Stephens MB (2018) Metamorphic zonation by out-of-sequence thrusting at back-stepping subduction zones: sequential accretion of the caledonian internides, Central Sweden. Tectonics. https://doi.org/10.1029/2018TC005088

Bender H, Glodny J, Ring U (2019) Absolute timing of Caledonian orogenic wedge assembly, Central Sweden, constrained by Rb–Sr multi-mineral isochron data. Lithos 344–345:339–359

Benowitz JA, Layer PW, Vanlaningham S (2014) Persistent long-term (c 24 Ma) exhumation in the Eastern Alaska Range constrained

by stacked thermochronology. Geol Soc Lond Spec Publ 378(1):225–243
Bergman S (1992) P-T paths in the Handöl area, central Scandinavia: record of Caledonian accretion of outboard rocks to the Baltoscandian margin. J Metamorph Geol 10:265–281
Bergman S (1993) Geology and geochemistry of mafic-ultramafic rocks (Köli) in the Handöl area, central Scandinavian Caledonides. Nor Geol Tidsskr 73:21–42
Bergman S, Sjöström H (1997) Accretion and lateral extension in an orogenic wedge: evidence from a segment of the Seve-Köli terrane boundary, central Scandinavian Caledonides. J Struct Geol 19:1073–1091
Brueckner HK, Cuthbert SJ (2013) Extension, disruption, and translation of an orogenic wedge by exhumation of large ultrahigh-pressure terranes: examples from the Norwegian Caledonides. Lithosphere 5:277–289
Brueckner HK, Van Roermund HL (2007) Concurrent HP metamorphism on both margins of Iapetus: ordovician ages for eclogites and garnet pyroxenites from the Seve Nappe Complex, Swedish Caledonides. J Geol Soc 164:117–128
Brueckner HK, Van Roermund HL, Pearson NJ (2004) An Archean (?) to Paleozoic evolution for a garnet peridotite lens with sub-Baltic shield affinity within the Seve Nappe Complex of Jämtland, Sweden, Central Scandinavian Caledonides. J Petrol 45:415–437
Brueckner HK, Carswell DA, Griffin WL, Medaris LG, Van Roermund HLM, Cuthbert SJ (2010) The mantle and crustal evolution of two garnet peridotite suites from the Western Gneiss Region, Norwegian Caledonides: an isotopic investigation. Lithos 117(1):1–19
Bruton DL, Lindström M, Owen AW (1985) The ordovician of scandinavia. In: Gee DG, Sturt BA (eds) The caledonide orogen-scandinavia and related areas. Wiley, Chichester, pp 273–282
Bukała M, Klonowska I, Barnes C, Majka J, Kośmińska K, Janák M, Fassmer K, Broman C, Luptáková J (2018) UHP metamorphism recorded by phengite eclogite from the Caledonides of northern Sweden: P-T path and tectonic implications. J Metamorph Geol 36(5):547–566
Chemenda AI, Mattauer M, Malavieille J, Bokun AN (1995) A mechanism for syn-collisional rock exhumation and associated normal faulting: results from physical modelling. Earth Planet Sci Lett 132(1):225–232
Chopin C (1984) Coesite and pure pyrope in high-grade blueschists of the Western Alps: a first record and some consequences. Contrib Mineral Petrol 86:107–118
Corfu F, Gasser D, Chew DM (2014) New Perspectives on the caledonides of scandinavia and related areas. Geol Soc Lond Spec Publ 390:718
Cuthbert S, Carswell D, Krogh-Ravna E, Wain A (2000) Eclogites and eclogites in the Western Gneiss region, Norwegian Caledonides. Lithos 52(1–4):165–195
Dallmeyer R (1990) $^{40}Ar/^{39}Ar$ mineral age record of a polyorogenic evolution within the Seve and Köli nappes, Trøndelag, Norway. Tectonophysics 179:199–226
Dallmeyer RD, Gee DG, Beckholmen M (1985) $^{40}Ar/^{39}Ar$ mineral age record of early Caledonian tectonothermal activity in the Baltoscandian Miogeocline, central Scandinavia. Am J Sci 285:532–568
Dazé A, Lee JK, Villeneuve M (2003) An intercalibration study of the Fish Canyon sanidine and biotite $^{40}Ar/^{39}Ar$ standards and some comments on the age of the Fish Canyon Tuff. Chem Geol 199:111–127
Di Vincenzo G, Carosi R, Palmeri R (2004) The relationship between tectono-metamorphic evolution and argon isotope records in white mica: constraints from in situ $^{40}Ar/^{39}Ar$ laser analysis of the Variscan basement of Sardinia. J Petrol 45(5):1013–1043
Dyrelius D (1985) A geophysical perspective of the Scandinavian Caledonides. In: Gee DG, Sturt BA (eds) The Caledonide orogen-scandinavia and related areas. Wiley, Chichester, pp 185–195
Essex R, Gromet L, Andréasson PG, Albrecht L (1997) Early Ordovician U–Pb metamorphic ages of the eclogite-bearing Seve nappes, Northern Scandinavian Caledonides. J Metamorph Geol 15:665–676
Fassmer K, Andersson B, Klonowska I, Walczak K, Froitzheim N, Majka J, Fonseca R (2017) Middle Ordovician subduction of continental crust in the Scandinavian Caledonides-an example from Tjeliken, Seve Nappe Complex, Sweden. Geophys Res Abstr 19:1460
Fossen H (2010) Extensional tectonics in the North Atlantic Caledonides: a regional view. Geol Soc Lond Spec Publ 335(1):767–793
Fossen H, Dunlap WJ (1998) Timing and kinematics of Caledonian thrusting and extensional collapse, southern Norway: evidence from $^{40}Ar/^{39}Ar$ thermochronology. J Struct Geol 20(6):765–781
Foster DA, Grice WC, Kalakay TJ (2010) Extension of the Anaconda metamorphic core complex: $^{40}Ar/^{39}Ar$ thermochronology and implications for Eocene tectonics of the northern Rocky Mountains and the Boulder batholith. Lithosphere 2:232–246
Gee DG (1975) A tectonic model for the central part of the Scandinavian Caledonides. Am J Sci 275:468–515
Gee DG (1978) Nappe displacement in the Scandinavian Caledonides. Tectonophysics 47:393–419
Gee DG (2015) Caledonides of Scandinavia, Greenland, and Svalbard, reference module in earth systems and environmental sciences. Elsevier Inc. https://doi.org/10.1016/B978-0-12-409548-909133-8, pp 1–15
Gee DG, Sturt BA (1985) The Caledonide orogen-Scandinavia and related areas. Wiley, Chichester, p 1266
Gee DG, Kumpulainen R, Roberts D, Stephens MB, Thon A, Zachrisson E (1985) Scandinavian Caledonides tectonostratigraphic map. Sveriges Geologiska Undersökning, scale 1:2,000,000
Gee DG, Fossen H, Henriksen N, Higgins AK (2008) From the early Paleozoic platforms of Baltica and Laurentia to the Caledonide Orogen of Scandinavia and Greenland. Episodes 31(1):44–51
Gee DG, Juhlin C, Pascal C, Robinson P (2010) Collisional orogeny in the Scandinavian Caledonides (COSC). GFF 132:29–44
Gee DG, Janák M, Majka J, Robinson P, van Roermund H (2013) Subduction along and within the Baltoscandian margin during closing of the Iapetus Ocean and Baltica-Laurentia collision. Lithosphere 5:169–178
Gee DG, Ladenberger A, Dahlqvist P, Majka J, Be'eri-Shlevin Y, Frei D, Thomsen T (2014) The Baltoscandian margin detrital zircon signatures of the central Scandes. In: Corfu F, Gasser D, Chew DM (eds) New perspectives on the caledonides of scandinavia and related areas. Geological Society, London, Special Publication 390, pp 131–155
Gee DG, Andréasson PG, Li Y, Krill A (2017) Baltoscandian margin, Sveconorwegian crust lost by subduction during Caledonian collisional orogeny. GFF 139(1):36–51
Gee DG, Klonowska I, Andréasson, P-G, Stephens MB (2020) Chapter 21: Middle thrust sheets in the Caledonide orogen, Sweden: The outer margin of Baltica, the continent–ocean transition zone and late Cambrian–Ordovician subduction–accretion. In: Stephens MB, Bergman Weihed J (eds) Sweden: lithotectonic framework, tectonic evolution and mineral resources. Geological Society, London, Memoirs 50, p 517–548 https://doi.org/10.1144/M50-2018-73
Gerya TV, Stöckhert B, Perchuk AL (2002) Exhumation of high-pressure metamorphic rocks in a subduction channel: a numerical simulation. Tectonics. https://doi.org/10.1029/2002TC001406
Gilio M, Clos F, van Roermund HLM (2015) The Friningen Garnet Peridotite (central Swedish Caledonides) A good example of

the characteristic PTt path of a cold mantle wedge garnet peridotite. Lithos 230:1–16
Gilotti JA, Jones KA, Elvevold S (2008) Caledonian metamorphic patterns in Greenland. In: Higgins AK, Gilotti JA, Smith MP (eds) The Greenland Caledonides: evolution of the northeast margin of Laurentia. Geological Society of America Memoir 202, pp 201–225
Gilotti JA, Kumpulainen R (1986) Strain softening induced ductile flow in the Särv thrust sheet, Scandinavian Caledonides. J Struct Geol 8(3):441–455
Giuntoli F, Menegon L, Warren CJ (2018) Replacement reactions and deformation by dissolution and precipitation processes in amphibolites. J Metamorph Geol 36(9):1263–1286
Giuntoli F, Menegon L, Warren CJ, Darling J, Anderson MW (2020) Protracted shearing at midcrustal conditions during large-scale thrusting in the Scandinavian Caledonides. Tectonics 39(9):e2020TC006267
Glodny J, Hierold J, Harms U (2017) Direct dating of ductile deformation within the Caledonian nappe stack: Rb-Sr mineral data and element mapping from the COSC-1 drill core. Geophys Res Abstr 19:6365
Gorbatschev R (1985) Precambrian basement of the Scandinavian Caledonides. In: Gee DG, Sturt BA (eds) The Caledonide Orogen-Scandinavia and related areas. Wiley, Chichester, pp 197–212
Grimmer JC, Glodny J, Drüppel K, Greiling RO, Kontny A (2015) Early- to mid-Silurian extrusion wedge tectonics in the central Scandinavian Caledonides. Geology 43(4):347–350
Gromet LP, Sjöström H, Bergman S, Claesson S, Essex RM, Andréasson PG, Albrecht L (1996) Contrasting ages of metamorphism in the Seve nappes: U–Pb results from the central and northern Swedish Caledonides. GFF 118:36–37
Guillot S, Hattori K, Agard P, Schwartz S, Vidal O (2009) Exhumation processes in oceanic and continental subduction contexts: a review. In: Lallemand S, Funiciello F (eds) Subduction zone geodynamics. Springer, Berlin, pp 175–205
Hacker BR, Gans PB (2005) Continental collisions and the creation of ultrahigh-pressure terranes: Petrology and thermochronology of nappes in the central Scandinavian Caledonides. Geol Soc Am Bull 117:117–134
Hacker BR, Gerya TV (2013) Paradigms, new and old, for ultrahigh-pressure tectonism. Tectonophysics 603:79–88
Hacker BR, Andersen TB, Johnston S, Kylander-Clark AR, Peterman EM, Walsh EO, Young D (2010) High-temperature deformation during continental-margin subduction & exhumation: the ultrahigh-pressure Western Gneiss Region of Norway. Tectonophysics 480:149–171
Harper DAT, Bruton DL, Rasmussen CMØ (2008) The Otta brachiopod and trilobite fauna: palaeogeography of Early Palaeozoic terranes and biotas across Baltoscandia. Fossils Strata 54:31–40
Jakob J, Andersen TB, Kjøll HJ (2019) A review and reinterpretation of the architecture of the south and south-central Scandinavian Caledonides—a magma-poor to magma-rich transition and the significance of the reactivation of rift inherited structures. Earth Sci Rev 192:513–528
Janák M, van Roermund H, Majka J, Gee D (2013) UHP metamorphism recorded by kyanite-bearing eclogite in the Seve Nappe Complex of northern Jämtland, Swedish Caledonides. Gondwana Res 23:865–879
Janák M, Ravna E, Majka J, Klonowska I, Kullerud K, Gee D, Froitzheim N (2017) Recent progress in recognition of UHP metamorphism in allochthons of the Scandinavian Caledonides (Seve Nappe Complex and Tromsø Nappe). Geophys Res Abstr 19:5161
Jiang D, Williams PF (1998) High-strain zones: a unified model. J Struct Geol 20(8):1105–1120
Karis L, Strömberg A (1998) Jämtlands Östliga Fjällberggrund: Beskrivning till Berggrundskartan över Jämtlands län: Del 2 Fjälldelen. Sveriges Geologiska Undersökning, Ser C 53(2):1–363
Kirkland C, Bingen B, Whitehouse M, Beyer E, Griffin W (2011) Neoproterozoic palaeogeography in the North Atlantic Region: inferences from the Akkajaure and Seve Nappes of the Scandinavian Caledonides. Precambr Res 186:127–146
Kjøll HJ, Andersen TB, Corfu F, Labrousse L, Tegner C, Abdelmalak MM, Planke S (2019) Timing of breakup and thermal evolution of a pre-Caledonian Neoproterozoic exhumed magma-rich rifted margin. Tectonics 38:1843–1862
Klonowska I, Majka J, Janák M, Gee DG, Ladenberger A (2014) Pressure–temperature evolution of a kyanite–garnet pelitic gneiss from Åreskutan: evidence of ultra-high-pressure metamorphism of the Seve Nappe Complex, west-central Jämtland, Swedish Caledonides. In: Corfu F, Gasser D, Chew DM (eds) New perspectives on the caledonides of scandinavia and related areas. Geological Society, London, Special Publication 390, pp 321–336
Klonowska I, Janák M, Majka J, Froitzheim N, Kośmińska K (2016) Eclogite and garnet pyroxenite from Stor Jougdan, Seve Nappe Complex, Sweden: implications for UHP metamorphism of allochthons in the Scandinavian Caledonides. J Metamorph Geol 34:p103-119
Klonowska I, Janák M, Majka J, Petrík I, Froitzheim N, Gee D, Sasinková V (2017) Microdiamond on Åreskutan confirms regional UHP metamorphism in the Seve Nappe Complex of the Scandinavian Caledonides. J Metamorph Geol 35:541–564
Krogh TE, Kamo SL, Robinson P, Terry MP, Kwok K (2011) U–Pb zircon geochronology of eclogites from the Scandian Orogen, northern Western Gneiss Region, Norway: 14–20 million years between eclogite crystallization and return to amphibolite-facies conditions. Can J Earth Sci 48(2):441–472
Kuiper K, Deino A, Hilgen F, Krijgsman W, Renne P, Wijbrans J (2008) Synchronizing rock clocks of Earth history. Science 320(5875):500–504
Kulling O (1933) Bergbyggnaden inom Björkvattnet-Virisenområdet i Västerbottensfjällens centrala del. Geologiska Föreningens i Stockholm Förhandlingar 55:167–422
Kumpulainen R (1980) Upper Proterozoic stratigraphy and depositional environments of the Tossåsfjället Group, Särv Nappe, southern Swedish Caledonides. Geologiska Föreningen i Stockholm Förhandlingar 102(4):531–550
Kylander-Clark AR, Hacker BR, Johnson CM, Beard BL, Mahlen NJ, Lapen TJ (2007) Coupled Lu–Hf and Sm–Nd geochronology constrains prograde and exhumation histories of high- and ultrahigh-pressure eclogites from western Norway. Chem Geol 242(1):137–154
Kylander-Clark AR, Hacker BR, Mattinson JM (2008) Slow exhumation of UHP terranes: titanite and rutile ages of the Western Gneiss Region, Norway. Earth Planet Sci Lett 272:531–540
Kylander-Clark AR, Hacker BR, Johnson CM, Beard BL, Mahlen NJ (2009) Slow subduction of a thick ultrahigh-pressure terrane. Tectonics 28(2):TC2003. https://doi.org/10.1029/2007TC002251
Ladenberger A, Be'eri-Shlevin Y, Claesson S, Gee D G, Majka J, Romanova IV (2014) Tectonometamorphic evolution of the Åreskutan Nappe–Caledonian history revealed by SIMS U–Pb zircon geochronology. In: Corfu F, Gasser D, Chew DM (eds) New perspectives on the Caledonides of Scandinavia and related areas. Geological Society, London, Special Publication 390, pp 337–368
Li B, Massonne HJ, Zhang J (2020) Evolution of a gneiss in the Seve nappe complex of central Sweden-Hints at an early Caledonian, medium-pressure metamorphism. Lithos 376:105746

Lin S, Jiang D, Williams PF (1998) Transpression (or transtension) zones of triclinic symmetry: natural example and theoretical modelling. Geol Soc Lond Spec Publ 135(1):41–57

Lin S, Jiang D, Williams PF (2007) Importance of differentiating ductile slickenside striations from stretching lineations and variation of shear direction across a high-strain zone. J Struct Geol 29(5):850–862

Lorenz H, Rosberg J-E, Juhlin C, Bjelm L, Almqvist BSG, Berthet T, Conze R, Gee DG, Klonowska I, Pascal C (2015) COSC-1-drilling of a subduction-related allochthon in the Palaeozoic Caledonide orogen of Scandinavia. Sci Drill 19:1–11

Ma C, Foster DA, Hames WE, Mueller PA, Steltenpohl MG (2019) From the Alleghanian to the Atlantic: extensional collapse of the southernmost Appalachian orogen. Geology 47(4):367–370

Ma C, Hames WE, Foster DA, Xiao W, Mueller PA, Steltenpohl MG (in press) Transformation of eastern North America from compression to extension in the Permian-Triassic. In: Whitmeyer SJ, Williams ML, Kellett DA, Tikoff B (eds) Laurentia: turning points in the evolution of a continent. Geological Society of America Memoir 220

Majka J, Be'eri-Shlevin Y, Gee DG, Ladenberger A, Claesson S, Konecny P, Klonowska I (2012) Multiple monazite growth in the Åreskutan migmatite: evidence for a polymetamorphic Late Ordovician to Late Silurian evolution in the Seve Nappe Complex of west-central Jamtland, Sweden. J Geosci 57(1):3–23

Majka J, Janák M, Andersson B, Klonowska I, Gee DG, Rosén Å, Kośmińska K (2014a) Pressure–temperature estimates on the Tjeliken eclogite: new insights into the (ultra)-high-pressure evolution of the Seve Nappe Complex in the Scandinavian Caledonides. In: Corfu F, Gasser D, Chew DM (eds) New perspectives on the caledonides of scandinavia and related areas. Geological Society, London, Special Publication 390, pp 369–384

Majka J, Rosén Å, Janák M, Froitzheim N, Klonowska I, Manecki M, Sasinková V, Yoshida K (2014b) Microdiamond discovered in the Seve Nappe (Scandinavian Caledonides) and its exhumation by the "vacuum-cleaner" mechanism. Geology 42(12):1107–1110

McDougall I, Harrison TM (1999) Geochronology and thermochronology by the $^{40}Ar/^{39}Ar$ method. Oxford, Oxford University Press, New York, p 269

Nilsson LP, Roberts D, Ramsay DM (2005) The Raudfjellet ophiolite fragment, Central Norwegian Caledonides: principal lithological and structural features. Norges Geologiske Undersøkelse Bull 445:101–117

Nystuen JP, Andresen A, Kumpulainen RA, Siedlecka A (2008) Neoproterozoic basin evolution in Fennoscandia, East Greenland and Svalbard. Episodes 31:35–43

Passchier CW, Trouw RAJ (2005) Microtectonics, 2nd edn. Springer, Berlin, p 366

Renne PR, Deino AL, Walter RC, Turrin BD, Swisher CC III, Becker TA, Curtis GH, Sharp WD, Jaouni AR (1994) Intercalibration of astronomical and radioisotopic time. Geology 22(9):783–786

Renne PR, Mundil R, Balco G, Min K, Ludwig KR (2010) Joint determination of ^{40}K decay constants and $^{40}Ar/^{40}K$ for the Fish Canyon sanidine standard, and improved accuracy for $^{40}Ar/^{39}Ar$ geochronology. Geochim Cosmochim Acta 74(18):5349–5367

Ring U, Glodny J (2010) No need for lithospheric extension for exhuming (U)HP rocks by normal faulting. J Geol Soc 167(2):225–228

Ring U, Will T, Glodny J, Kumerics C, Gessner K, Thomson S, Güngör T, Monié P, Okrusch M, Drüppel K (2007) Early exhumation of high-pressure rocks in extrusion wedges: Cycladic blueschist unit in the eastern Aegean, Greece, and Turkey. Tectonics. https://doi.org/10.1029/2005TC001872

Roberts D, Nordgulen Ø, Melezhik V (2007) The Uppermost Allochthon in the Scandinavian Caledonides: from a Laurentian ancestry through Taconian orogeny to Scandian crustal growth on Baltica. In: Hatcher RD, Carlson MP, McBride JH, Catalán JRM (eds) 4-D Framework of continental crust. Geological Society of America Memoir 200, pp 357–377

Root D, Corfu F (2012) U–Pb geochronology of two discrete Ordovician high-pressure metamorphic events in the Seve Nappe Complex, Scandinavian Caledonides. Contrib Miner Petrol 163(5):769–788

Röshoff K (1978) Structures of the Tännäs Augen Gneiss Nappe and its relation to under- and overlying units in the central Scandinavian Caledonides. Sveriges Geologiska Undersökning C 739:1–35

Samson SD, Alexander EC (1987) Calibration of the interlaboratory $^{40}Ar/^{39}Ar$ dating standard MMhb-1. Chem Geol 66(1–2):27–34

Seranne M (1992) Late Paleozoic kinematics of the Møre-Trøndelag Fault Zone and adjacent areas, central Norway. Norsk Geologisk Tidsskriftv 72:141–158

Sjöstrand T (1999) Bedrock map 19C Storlien SO. Sveriges geologiska undersökning Ai 109, scale 1:50 000, 1 sheet

Sjöström H (1984) The Seve-Köli Nappe Complex of the Handöl-Storlien-Essandsjøen area, Scandinavian Caledonides. Geologiska Föreningen i Stockholm Förhandlingar 105(2):93–118

Sjöström H, Talbot C, Bergman S (1996) The development of antiformal windows in the central Scandinavian Caledonides: antiformal stacks modified by extensional detachments. GFF 118(S4):40–40. https://doi.org/10.1080/11035899609546313

Smith DC (1984) Coesite in clinopyroxene in the Caledonides and its implications for geodynamics. Nature 310(5979):641–644

Sobolev N, Shatsky V (1990) Diamond inclusions in garnets from metamorphic rocks: a new environment for diamond formation. Nature 343(6260):742

Solli A, Nordgulen Ø (2008) Bedrock map of Norway and the Caledonides in Sweden and Finland. Geological Survey Norway, scale: 1: 2,000,000, 1 sheet

Spell TL, McDougall I (2003) Characterization and calibration of $^{40}Ar/^{39}Ar$ dating standards. Chem Geol 198(3–4):189–211

Spencer KJ, Hacker BR, Kylander-Clark AR, Andersen TB, Cottle JM, Stearns MA, Poletti JE, Seward GG (2013) Campaign-style titanite U–Pb dating by laser-ablation ICP: Implications for crustal flow, phase transformations and titanite closure. Chem Geol 341:84–101

Spengler D, Brueckner HK, van Roermund HL, Drury MR, Mason PR (2009) Long-lived, cold burial of Baltica to 200 km depth. Earth Planet Sci Lett 281(1–2):27–35

Steiger RH, Jäger E (1977) Subcommission on geochronology: convention on the use of decay constants in geo-and cosmochronology. Earth Planet Sci Lett 36(3):359–362

Stephens MB, Van Roermund HL (1984) Occurrence of glaucophane and crossite in eclogites of the Seve Nappes, southern Norrbotten Caledonides, Sweden. Norweg J Geol 61:155–163

Strömberg AG (1961) On the tectonics of the Caledonides in the southwestern part of the county of Jämtland, Sweden. Bull Geol Inst Univ Uppsala 39:1–92

Sturt BA, Ramsay DM, Neuman RB (1991) The Otta Conglomerate, the Vågåmo Ophiolite−further indications of early Ordovician Orogenesis in the Scandinavian Caledonides. Norsk Geologisk Tidsskrif 71:107–115

Svenningsen OM (2001) Onset of seafloor spreading in the Iapetus Ocean at 608 Ma: precise age of the Sarek Dyke Swarm, northern Swedish Caledonides. Precambr Res 110(1):241–254

Thompson AB, Schulmann K, Jezek J (1997) Extrusion tectonics and elevation of lower crustal metamorphic rocks in convergent orogens. Geology 25(6):491–494

Törnebohm A (1888) Om fjällproblemet. Geologiska Föreningen i Stockholm Förhandlingar 10(5):328–336

Tucker RD, Robinson P, Solli A, Gee DG, Thorsnes T, Krogh TE, Nordgulen Ø, Bickford M (2004) Thrusting and extension in the Scandian hinterland, Norway: new U–Pb ages and tectonostratigraphic evidence. Am J Sci 304(6):477–532

Van Roermund H (1985) Eclogites of the Seve nappe, central Scandinavian Caledonides. In: Gee DG, Sturt BA (eds) The Caledonide Orogen-Scandinavia and related areas. Wiley, Chichester, pp 873–886

Van Roermund H (1989) High-pressure ultramafic rocks from the allochthonous nappes of the Swedish Caledonides. In: Gayer RA (ed) The Caledonide geology of scandinavia. Graham & Trotman, London, pp 205–219

Villa I (1998) Isotopic closure. Terra Nova 10:42–47

Walczak K, Majka J, Klonowska I, Barnes C (2019) Two distinct high grade metamorphic events at c 500 Ma and 450 Ma recorded in zircon from the Snasahögarna diamond-bearing gneiss, Scandinavian Caledonides. Geophys Res Abstr 21:6945

Walczak K, Barnes CJ, Majka J, Gee DG, Klonowska I (2022) Zircon age depth-profiling sheds light on the early Caledonian evolution of the Seve Nappe Complex in west-central Jämtland. Geosci Front 13(2):101112. https://doi.org/10.1016/j.gsf.2020.11.009

Walsh EO, Hacker BR, Gans PB, Wong MS, Andersen TB (2013) Crustal exhumation of the Western Gneiss Region UHP terrane, Norway: $^{40}Ar/^{39}Ar$ thermochronology and fault-slip analysis. Tectonophysics 608:1159–1179

Warren C (2013) Exhumation of (ultra-) high-pressure terranes: concepts and mechanisms. Solid Earth 4(1):75–92

Yamato P, Burov E, Agard P, Le Pourhiet L, Jolivet L (2008) HP-UHP exhumation during slow continental subduction: Self-consistent thermodynamically and thermomechanically coupled model with application to the Western Alps. Earth Planet Sci Lett 271(1–4):63–74

York D, Hall CM, Yanase Y, Hanes JA, Kenyon WJ (1981) $^{40}Ar/^{39}Ar$ dating of terrestrial minerals with a continuous laser. Geophys Res Lett 8(11):1136–1138

Young DJ (2017) Structure of the (ultra) high-pressure Western Gneiss Region, Norway: Imbrication during Caledonian continental margin subduction. Geol Soc Am Bull 130(5–6):926–940

Young DJ, Hacker BR, Andersen TB, Corfu F (2007) Prograde amphibolite facies to ultrahigh-pressure transition along Nordfjord, western Norway: Implications for exhumation tectonics. Tectonics 26(1):TC1007. https://doi.org/10.1029/2004TC001781

Zachrisson E (1973) The westerly extension of Seve rocks within the Seve-Köli Nappe Complex in the Scandinavian Caledonides. Geologiska Föreningen i Stockholm Förhandlingar 95(2):243–251